A REPORT

to

THE NATIONAL AERONAUTICS AND SPACE ADMINISTRATION

on

The Research Progress Of

Grant NsG 708

on

BASIC RESEARCH IN SEMICONDUCTOR DETECTOR-DOSIMETER CHARACTERISTICS, AS APPLIED TO THE PROBLEMS OF WHOLE BODY DOSIMETRY

from

George W. Crawford
Professor of Physics

SOUTHERN METHODIST UNIVERSITY
DALLAS, TEXAS 75222

September, 1966

Annual Progress Report

NsG 708

I. Experimental Progress

A. Lithium Drifted Silicon Semiconductor Detectors:

1. Seventy different detectors have been incorporated into this study. They represent a family of various sized devices ranging in size from 1 x 1 x 1 mm to 7 x 7 x 150 mm. Long detectors, i.e., having proton path lengths in silicon of 10, 20, 30, 50, 70, 100, 120, 130 and 150 mm are being used to totally absorb high energy protons. Shorter path lengths are used to measure stopping power $dE/\rho dX$ in silicon.
2. Lithium-drifted detectors of special shapes and sizes are fabricated at SMU. New techniques of fabrication, mounting and encapsulation were developed.
3. Combinations of detectors have been developed to permit simultaneous measurements of dE/dx and E with identification of both mass and energy of the incident particle for translation to a surface dose and depth dose distribution.

B. Charge-pulse response of silicon detectors:

The charge-pulse response of many of the detectors have been measured for the proton energies listed in D. as a function of proton energy, proton path length in silicon and operating conditions of the detector. The average energy required to produce an ion-electron pair has been measured from both the stopping power measurements in silicon and from the protons totally absorbed in silicon. These data are required to translate the current from each detector produced by a known radiation flux density and stored in a calibrated condenser into dose, i.e., the total energy absorbed per unit mass of silicon.

C. Detector Life-time Behavior Studies:

The depletion depth, volume, noise level, charge pulse per Mev, dark current and capacitance are being measured for each detector used in the study. The complete age-usage history thus obtained over the two year period will be used to a) predict the usable life of a detector and b) to pin-point and predict loss of reliability of data produced by the detector.

D. Stopping Power Measurements:

Data has been taken using protons having energies of 5, 6, 8, 10, 11, 12, 13, 14, 15, 16, 36, 37, 40, 100, 160, and 187 Mev. Absorbers were used in duplicate sets of three different thicknesses permitting measurements on six different absorbers with each of two or more detectors.

a. Elements: Al, Be, C, Cu, Fe, Pb, Si
b. Plastics: Nylon, plexiglass, polyethylene, tissue equivalent.
c. Tissue: Bone, muscle, fat.

E. Field Trips:

1. to the University of Texas, Austin, Texas
   Dates: October 10-11, 1964
   Accelerator time: 36 hours
   Proton Energies 5-14 Mev

   Dates: December 28-29, 1964
   Accelerator time: 36 hours
   Proton Energies 8-16 Mev

2. Oak Ridge National Laboratories, Oak Ridge, Tennessee
   Dates: November 21-29, 1964
   Accelerator time: 80 hours
   Proton Energies: 36-40 Mev

3. University of Uppsala, Uppsala, Sweden
   Dates: October 23-November 8, 1964
   Accelerator time: 100 hours
   Proton Energy: 187 Mev

4. University of Southern California, Los Angeles, California
   Dates: May 20-22, 1965
   Accelerator time: 24 hours
   Proton Energies: 21-30 Mev

5. McGill University, Montreal, Canada
   Dates: August 4-15, 1965
   Accelerator time: 110 hours
   Proton Energy: 100 Mev

6. Harvard University, Cambridge, Mass.
   Dates: August 16-19, 1965 NOTE: Cyolotron main generator failed just before SMU turn to "go on the beam." This major breakdown forced rescheduling field trip to
   Dates: January 18-24, 1966
   Accelerator time: 84 hours
   Proton Energy: 160 Mev

7. University of Uppsala, Uppsala, Sweden
   Dates: April 20-May 4, 1966
   Accellerator time: 138 hours
   Proton Energies 185.6 Mev

8. University of Uppsala, Uppsala, Sweden
   Dates: June 9-July 8, 1966
   Accelerator time: 166 hours
   Proton Energies 185.6 Mev.

F. NASA Participation:

Members of the NASA, Manned Space Center, Space Radiation and Fields Branch participated in the research effort at the University of Uppsala, at Oak Ridge National Laboratory, and at McGill University. At each facility additional research of special interest to this Branch were accomplished. These included exposure of nuclear track plate emulsions and calibration of various dosimeters. The accelerator time made available to NASA at no charge ranged from 10 to 24 hours at each facility.

II. Theoretical Progress

A. Linear Stopping Power Calculations:

A program for calculating linear stopping power, $dE/\rho dx$; based on the Bethe-Block equation

$$-\frac{dE}{\rho dx} = \frac{0.1536Z}{\beta^2 A}\left[\ell n\ \frac{2\ mc^2\beta^2}{1-\beta^2} - \beta^2 - \ell n\ I - \frac{\Sigma Ci}{Z}\right]$$

including shell corrections has been completed, tested and used on the SMU, CDC-3400 computer to calculate the correct thicknesses for the pure elements. The mean ionization potential, I, has been evaluated experimentally for each element.

B. Monte Carlo Stopping Power Calculations:

The linear stopping power program has been incorporated into a Monte Carlo transport program which permits Coulomb interaction with both the orbital electrons and the nuclei. This program has been used to verify the stopping power measurement and the energy straggle measured experimentally. For porton energies below 200 Mev and $\rho dx > 0.75$ g/cm^2, the difference between the linear value and the Monte Carlo values of the loss of energy is given by $0.2555\ \beta^2(1-\beta^2)$ where $\beta = v/c$ for the proton.

C. Determination of Z/A and I for complex absorbers:

The above programs are being used to determine effective Z, A, and I values for water, bone, meat and fat based on the experimental stopping power measurements. The end result will be a program by which dose, i.e., the total energy absorbed per unit mass of the absorbing material, can be calculated as a function of flux density, type and energy of the ionizing radiation.

D. Calculation of Effective Z/A, and I.:

The effective values of Z/A, and I for each of four plastics studied are being used to obtain a mathematical model for calculating these quantities where the chemical composition and relative abundance of a heterogeneous material is known.

E. Dose Calculation

The computer program is being written to permit calculation of a depth dose distribution in a multilayer, i.e., skin, muscle, bone fat, etc., absorber in a heterogeneous radiation environment. Other options permit a) the particles to enter everywhere over the surface of the "absorber"; b)determination of energy lost in transit through the absorber; c) energy and angular distribution of secondary radiations (nuclear or orbital electrons) to permit study of reabsorption or escape from site of dose interest and d) the absorber to have a complex geometry.

F. Correlation Between Biological Response and Dose Measurement:

The final step is the determination of a biological response of the chosen subject to the actual (if on a mission) or the predicted radiation environment. Indicative predictions are possible on the basis of human cancer cases and animal irradiations. The biological response itself is a medical study and the responses used in this analysis will be from well qualified sources. The precise determination of the radiation environment which produced the response is a physical study. Translating the laboratory radiation environment into terms of a space radiation environment and correlating the biological response to the space radiation exposure is one of the goals of this research effort.

The main goal of this project is to provide the basic physical data concerning silicon detectors and the true mathematical path to permit the physical measurement or sequence of measurements made with a silicon detector so that the silicon dose and LET measurements can be translated directly into tissue dose and depth dose distribution. It is from these translations that indicative predictions of the biological response can be made.

The data currently being used is that provided by Dr. Borje Larsson from his studies based on his treatment of human cancers using irradiation by 187 Mev protons for treatment and the whole body irradiations of primates by the Bionucleonics Division of the USAF School of Aerospace Medicine. Other studies will be included when it is possible to obtain enough information concerning the laboratory radiation environment to permit a direct translation of the dosimetry into NASA-SMU dosimetry.

III. Funding:

A. NASA

	1964-65	1965-66	1966-67	Total
1. Direct Costs	$71,262.00	$43,333.34	$35,898.00	$150,493.34
2. Overhead	5,506.74	8,666.66	11,059.00	25,232.40
Total	$76,768.74	$52,000.00	$46,957.00	$175,725.74

The total NASA contribution is $175,725.74.

B. Other Universities:
The following cyclotron grants were made to SMU for this project:

Granting Univ.	Accelerator Time	Estimated Cost
University of Texas	36 hours	$ 1,080.
Oak Ridge Nat'l Lab.	80 hours	2,000.
McGill University	110 hours	5,500.
Harvard University	84 hours	1,400.
Uppsala University	404 hours	24,220.
Total		$34,200.

The total contribution in free accelerator time is about $34,200.00.

C. Using Government guidelines, it was possible to show that SMU actually gave matching funds in terms of computer time and salary in the amount of $26,444.00 for the first two years and so far has given $9,300 in computer time in June, July, August, 1966.

D. The total financial support for the entire three year period: $247,000.00.

IV. Personnel:

	No. employed each of the three, one-year periods.			Total No. of different men.
	1964-65	1965-66	1966-67	
Faculty	1	2	3	3
Non-Faculty	2	1	3	3
Graduate Assistants	5	6	5	8
Undergraduate Assts.	3	3	1	6
Total	11	12	12	20

V. Publications

A. The Following Technical Papers Were Given as Listed Below.

At the Sixty-Eighty Annual Meeting of the Texas Academy of Science, Abilene, Texas, December, 1964.

1. Cummins, J. R. — Preliminary Report of the Experimental Determination of I_{eff}, Z_{eff}, and A_{eff} in the Bethe-Bloch Stopping Power Equation for Four Plastics.
2. Crawford, G. W. — Linear and Monte Carlo Calculations of Stopping Power and Energy Straggle
3. Nipper, Daniel C. — Stopping Power Measurements of Al, Cu, and Si Using 36.1 MeV Protons.
4. Snow, B. D. — The Preparation of Lithium-Drifted Solid State Radiation Detectors.

At the American Physical Society Meeting, Honolulu, Hawaii, September, 1965.

1. Crawford, G. W. — Linear and Monte Carlo Calculations of Stopping Power and Energy Straggle.

At the Sixty-Ninth Annual Meeting of the Texas Academy of Science, Dallas, Texas, December, 1965.

1. Crawford, G. W. — Operating Characteristics of Very Long Silicon Detectors.
2. Snow, B. D. — Fabrication of Very Long Silicon Detectors.

Respectfully submitted,

George W. Crawford

George W. Crawford
Professor of Physics
Southern Methodist University

Appendix A

PREPARATION OF LITHIUM-DRIFTED SEMICONDUCTOR NUCLEAR PARTICLE DETECTORS

To

THE NATIONAL AERONAUTICS AND SPACE ADMINISTRATION

for

NsG 708

A GRANT IN SUPPORT

of

BASIC RESEARCH IN SEMICONDUCTOR DETECTOR-DOSIMETER CHARACTERISTICS, AS APPLIED TO THE PROBLEMS OF WHOLE BODY DOSIMETRY

from

SOUTHERN METHODIST UNIVERSITY
Dallas, Texas 75222

October, 1966

TABLE OF CONTENTS

LIST OF TABLES

LIST OF ILLUSTRATIONS

LIST OF ILLUSTRATIONS--(Cont'd.)

INTRODUCTION

The process for preparing lithium drifted "p-i-n" detectors was conceived and developed by E. M. Pell[1] of General Electric Research Laboratory in 1959. By this method lithium was diffused into "p" type silicon to form an "n-p" junction diode. A reverse bias was applied to this diode which was held at a sufficiently elevated temperature to give the lithium donor ions appreciable mobility but low enough to prevent flooding.[2,3] While in this condition the lithium ions drifted under the influence of the electric field and diffusion current to compensate the boron ions in the "p" region.[4] Thus, this region became depleted of free carriers and the depletion continued to spread as long as the temperature and biasing voltage were maintained.[5] Depletion widths as wide as 5 mm were formed.

For practical purposes this compensated region was intrinsic in the sense that the electron and hole concentration were equal. Consequently, an "n-i-p" formation was accomplished with the width of the intrinsic region depending upon the drift parameters.[6]

During detector operation a bias, positive from "n" to

"p," depleted the free carriers from the compensated region. The resulting intrinsic region became the sensitive region for particle detection. This depleted layer was, in effect, a layer of extremely high resistance material separating opposite electric charges. An appreciable capacitance resulted which varied with depletion width and, consequently, voltage.[7]

A particle incident on the sensitive region of the biased detector transferred its energy to the silicon by forming electron-hole pairs. These carriers were swept out of the intrinsic layer by the strong electric field and collected by the "plates" of the diode capacitor. The flow of electrons and holes were additive to constitute an electric current. A voltage pulse was produced when this current passed through a load resistor in the applicable circuitry. Each pulse was stored in electronic equipment to give a measure of the energy lost by the incident particle.[8]

For meaningful resolution of data similar to those above, a low noise to signal (pulse) ratio must be maintained. A detector capable of completely absorbing 200 Mev protons with a very low noise to signal ratio and good charge collection properties was required for the research project of which the work reported here was a part.

THEORY

The theory associated with the preparation of lithium drifted silicon detectors may be divided into five parts: (1) Theory of basic material; (2) Theory of diffusions; (3) Theory of "p-n" junctions; (4) Theory of drift; and (5) Theory of operation.

Theory of Basic Material

A semiconductor is defined by an electrical conductivity that is intermediate between that of an insulator and that of a metal. The classification is as follows:

Insulators: 10^{-22} to 10^{-14} mho-cm^{-1}

Semiconductors: 10^{-9} to 10^{2} mho-cm^{-1}

Conductors: 10^{5} mho-cm^{-1} and greater

When free electrons are perturbed by a periodic potential arising from the periodic crystal lattice, it is shown by second order degenerate perturbation theory that there is a "gap" between adjacent energy levels.[10,11] There can exist N energy levels, where N is the number of unit cells in a crystal, in each energy band. But two electrons can occupy each level if their spins are anti-parallel. Thus, each energy band can hold 2 N electrons.[12]

In general elements with an even number of electrons/unit cell will not be conductors since the energy bands would be full and additional energy would be required to excite them into the next available energy band. Similarly, elements with an odd number of electrons/unit cell would be conductors. However, not all elements with an even number of electrons/unit cell are poor conductors because of band overlap.

Silicon has four conduction electrons and the energy gap, E_G, is intermediate between conductors and insulators classifying it as a semiconductor. The energy level diagram for silicon is shown in Figure 1 with E_G = 1.21 ev at 0°K and conductivity σ = 3.3×10^{-6} mho cm^{-1}.[13]

The Fermi-Dirac distribution function, f(E), which gives the probability that a quantum state with energy E is occupied by an electron, is given by the formula[14]

$$f(E) = \frac{1}{1 + e^{(E - E_F)/kT}} \qquad (1)$$

where E_F is the Fermi energy or band and is the energy at which the probability of a state being filled is one-half,[15] k is Boltzmann's constant and T is the absolute temperature. Using free electron theory the temperature dependency of E_F is given approximately by[16]

$$E_F \approx E_F(0)\left[1 - \frac{\pi^2}{12}\left(\frac{kT}{E_F(0)}\right)^2\right] \qquad (2)$$

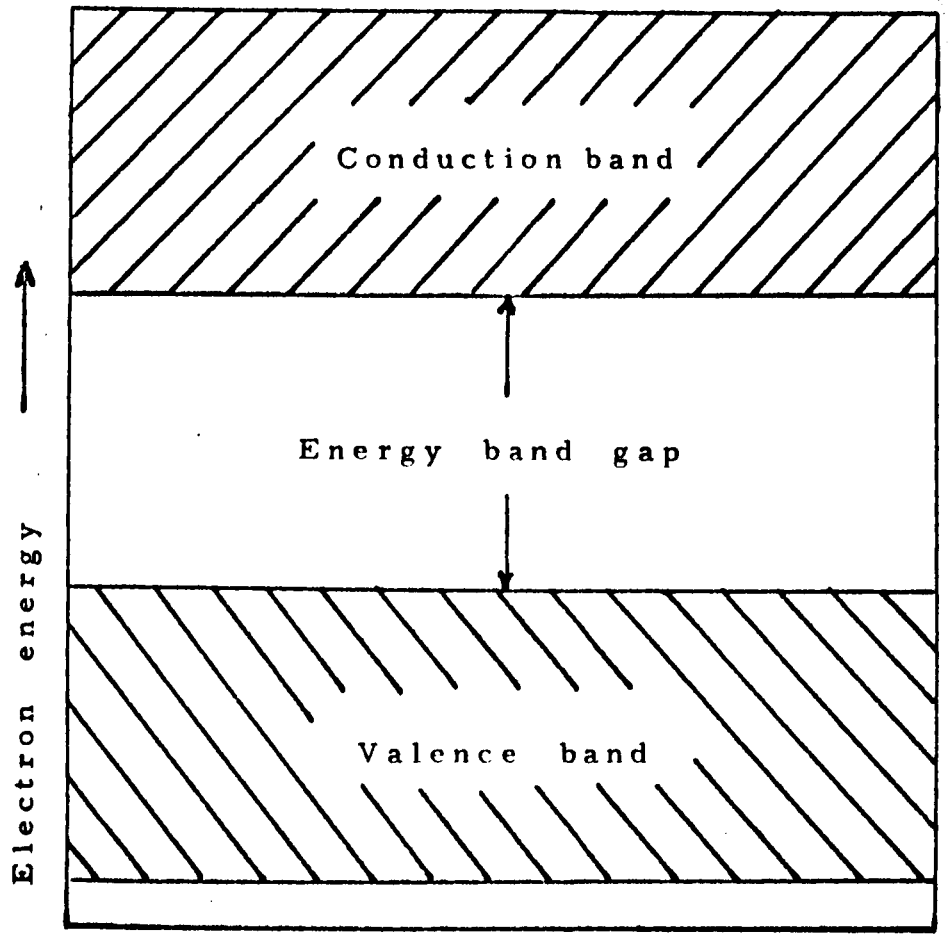

Fig. I. Energy-level diagram for Silicon

where $E_F^{(0)}$, the Fermi energy at $0^\circ K$, is

$$E_F^{(0)} = \frac{\hbar^2}{2m}(3\pi^2 n^{(0)})^{2/3}. \qquad (3)$$

$n^{(0)}$ is the charge carrier concentration at $0^\circ K$. Diagrams of the Fermi-Dirac distribution functions superimposed on energy-band diagrams are shown in Figure II.[17]

The value of kT at $T = 300^\circ K$ is 0.026 ev and the value of E_G at $300^\circ K$ is 1.1 ev.[17] The energy difference between the conduction band and the Fermi level $(E_C - E_F)$ is 0.55 ev. For this situation, where $E - E_F \gg kT$, $f(E)$ may be expressed as

$$f(E) \approx e^{-(E-E_F)/kT}. \qquad (4)$$

Equation (4) gives the value of that fraction of the quantum states at energies E occupied by an electron. Hence, $1 - f(E)$ corresponds to the fraction of states left vacant when the electron enters the conduction band that leaves behind a hole. From Equation (1)

$$1 - f(E) = 1 - \frac{1}{1 + e^{(E-E_F)/kT}} \qquad (5)$$

$$1 - f(E) = \frac{1 + e^{(E-E_F)/kT} - 1}{1 + e^{(E-E_F)/kT}} \qquad (6)$$

$$1 - f(E) = \frac{e^{(E-E_F)/kT}}{1 + e^{(E-E_F)/kT}} \qquad (7)$$

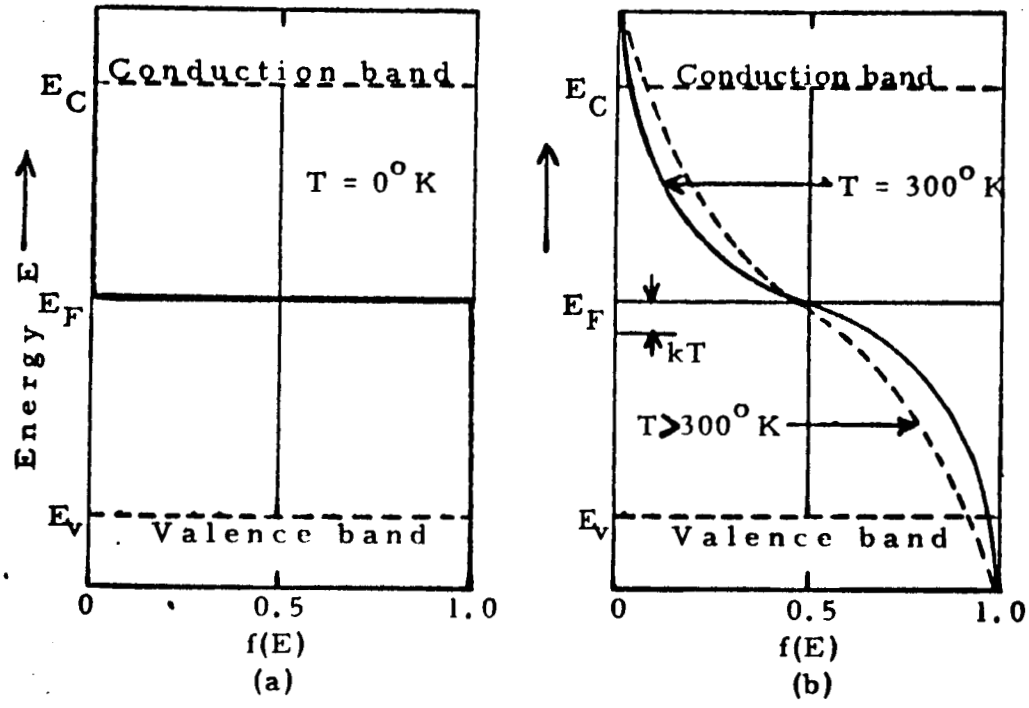

Fig. II. Fermi-Dirac distribution functions superimposed on energy-band diagrams.

$$1 - f(E) = \frac{1}{\frac{1}{e^{(E-E_F)/kT}} + 1} \qquad (8)$$

$$1 - f(E) = \frac{1}{1 + e^{(E - E_F)/kT}} \qquad (9)$$

making the same approximation as in Equation (4); i.e., $E_F - E_V \gg kT$ yields

$$1 - f(E) \approx e^{-(E_F - E)/kT}. \qquad (10)$$

Defining $g(E)$ as the number of quantum states per unit energy per unit volume of the crystal, the density of states N in a particular energy range $E + dE$ would be

$$N = g(E)\, dE. \qquad (11)$$

Therefore, the density of free carriers would be given by

$$n = \int_{E_1}^{E_2} f(E)\, g(E)\, dE. \qquad (12)$$

By Brillouin-Zone analysis, the derived expression for $g(E)$ is[18]

$$g(E) = \frac{1}{2\pi^2}\left(\frac{2m_e}{\hbar^2}\right)^{3/2} (E - E_1)^{1/2} \qquad (13)$$

The density of electrons in the conduction band is then

$$n = \int_{E_C}^{\infty} e^{-(E - E_F)/kT} \frac{1}{2\pi^2}\left(\frac{2m_e}{\hbar^2}\right)^{3/2} (E - E_C)^{1/2} dE. \qquad (14)$$

Integrating beyond the top of the conduction band causes very little error.

Letting $E_1 = E - E_C$,

$$n = e^{-(E_C - E_F)/kT} \frac{1}{2\pi^2}\left(\frac{2m_e}{\hbar^2}\right)^{3/2} \int_o^{\infty} E_1^{1/2} e^{-\frac{E_1}{kT}} dE_1, \quad (15)$$

which yields

$$n = 2\left(\frac{2\pi m_e kT}{h^2}\right)^{3/2} e^{-(E_C - E_F)/kT}. \quad (16)$$

Defining

$$N_C = 2\left(\frac{2\pi m_e kT}{h^2}\right)^{3/2}, \quad (17)$$

$$n = N_C e^{-(E_C - E_F)/kT}. \quad (18)$$

Similarly

$$p = 2\left(\frac{2\pi m_h kT}{h^2}\right)^{3/2} e^{-(E_F - E_V)/kT}. \quad (19)$$

Defining

$$N_V = 2\left(\frac{2\pi m_h kT}{h^2}\right)^{3/2}, \quad (20)$$

$$p = N_V e^{-(E_F - E_V)/kT}. \quad (21)$$

Multiplying (18) by (21) yields

$$np = 4\left(\frac{2\pi kT}{h^2}\right)^3 (m_e m_h)^{3/2} e^{-\frac{E_g}{kT}}, \qquad (22)$$

where

$$E_g = E_C - E_V. \qquad (23)$$

It is therefore evident that the product, np, is independent of the Fermi level, E_F. Furthermore, it is dependent only on temperature and is a constant for any given temperature. Experimental measurements of high-quality silicon crystals have yielded the following empirical expression.[19,20]

$$np = 15 \times 10^{32} T^3 e^{-1.21/kT} \qquad (24)$$

In intrinsic silicon carriers are due to thermal excitation and n = p. Therefore,

$$n_i^2 = p_i^2 = np \qquad (25)$$

When electrons became thermally excited and enter the conduction band, an equal number of holes are left in the valence band for conduction. Hence, conductivity increases until the carrier population is great enough for lattice vibrations to impede movement of the carriers. The conductivity due to thermally generated holes and electrons in intrinsic silicon is termed intrinsic conduction.

A two dimensional picture of a silicon crystal showing only

the valence covalent bonding electrons[21] is shown in Figure III. The Fermi-Dirac distribution function superimposed on the energy-band diagrams for this crystal is given in Fig. II.

Suppose now a group III impurity is introduced and displaces one of the silicon atoms. There will be an electron deficiency or a "hole" which acts like a positive charge to readily accept a free electron from the crystal. Consequently, group III impurities are called acceptor impurities.

If a silicon atom is displaced by a group V atom four of the five valence electrons will satisfy the covalent bonding structure. However, the fifth electron is relatively free to migrate through the crystal. For this reason group V atoms are termed donor impurities.

Each of the above "doping" atoms, as they are called, are defined as displacement atoms. An atom may be positioned interstitually, that is, in the space between lattice atoms. They are, therefore, called interstitial atoms. Lithium is such an atom[22,23] and "gives up" an electron to the silicon crystal to act as a donor impurity.

The presence of impurities will modify slightly the distribution of quantum states within the crystal. At very low temperatures, where the excess electrons are bound to the donor atoms, each donor atom will remove a state from the conduction band and

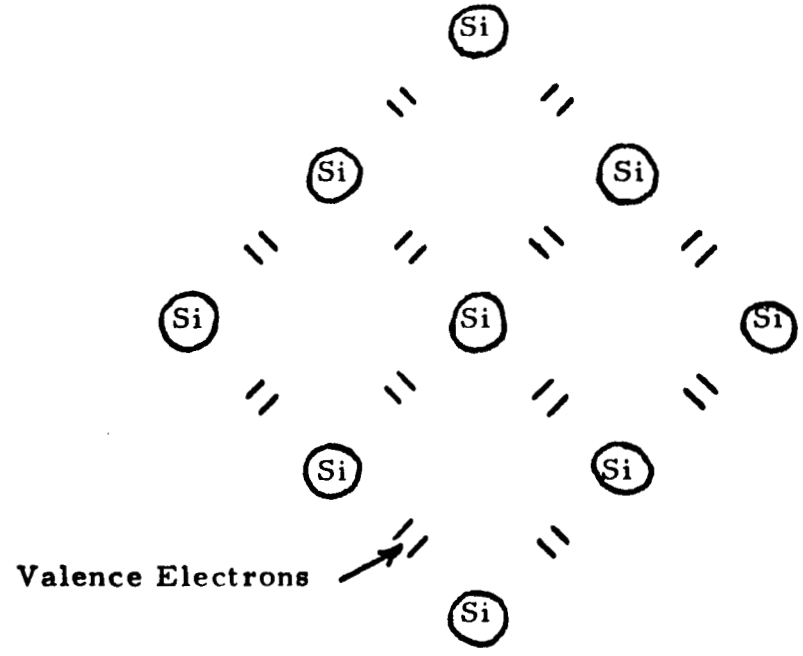

Fig. III. Two dimensional covalent bonding picture of a Silicon crystal.

establish it as an allowed state of lower energy. This lower energy level is referred to as the donor impurity energy level, E_D, and is below the bottom of the conduction band by an amount equal to the donor ionization energy. Similarly, for an acceptor impurity, each atom elevates a state from the valence band to an acceptor impurity energy level, E_A, just equal to the acceptor ionization energy.[24] These energy levels are illustrated in Fig. IV.

Material with an excess of donor impurities ($N_D > N_A$) is called "n" type because conduction is due to negative charge carriers or electrons in the conduction band. Similarly, material with an excess of acceptor impurities ($N_A > N_D$) is called "p" type because conduction is due to an excess of hole carriers in the valence band acting like positive charges. If $N_D = N_A$, the conduction is intrinsic, and the crystal is said to be compensated. In an "n" type semiconductor, the electrons are called majority carriers and holes minority carriers. Likewise, in "p" type material, the holes are the majority carriers and electrons minority carriers. Conduction due to added impurities is termed extrinsic conduction.

When $N_D > N_A$ at room temperature there is a high occupancy of the allowed states in the conduction band and a low occupancy of holes in the valence band. The conduction where $N_A > N_D$ has opposite effects. It is clear that the Fermi level, which is a

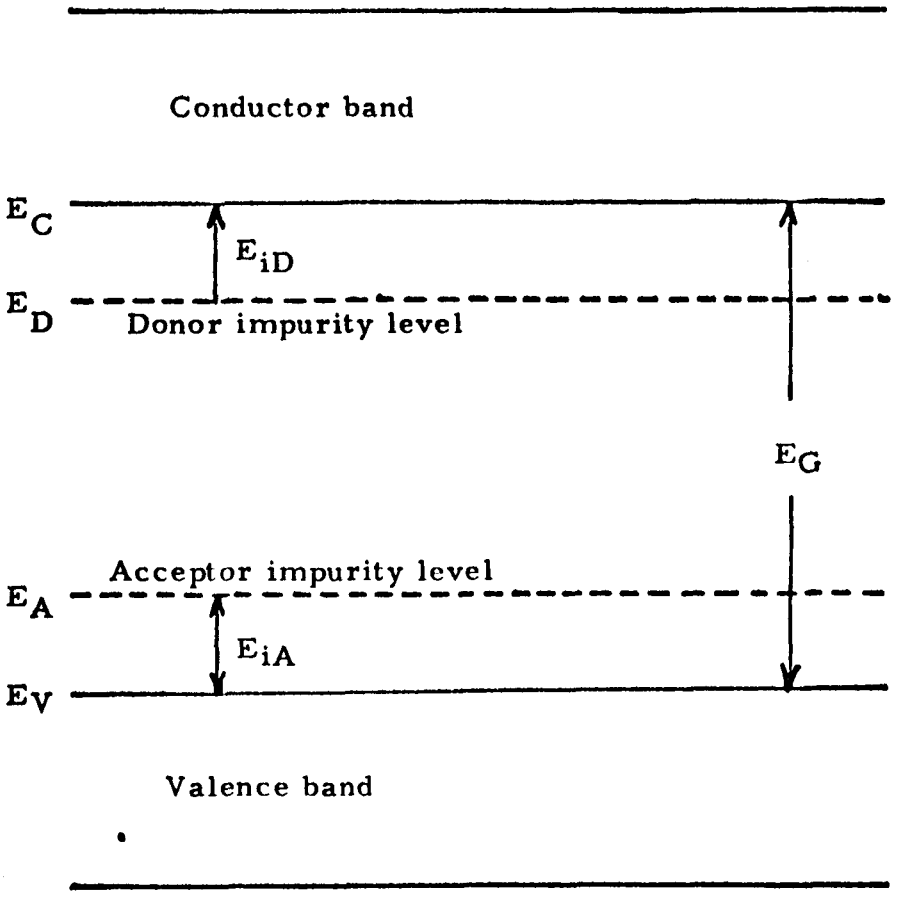

Fig. IV. Energy-level diagram for impurity semiconductor.

measure of the probability of occupancy of the allowed states,[25] will be affected. The positions of the Fermi level for impurity semiconductors are shown in Fig. V.

It has been theorized, and demonstrated by experiment, that certain allowed energy states can and do exist in the region of the forbidden-energy band. These states are called recombination centers and are attributed to foreign impurities or perhaps structural defects in the crystal. A state of this nature may exist anywhere in the forbidden region dependent on the impurity. The action of the center is to capture either a free electron from the conduction band or an electron from the valence band, leaving a hole behind. Likewise, the filled center may be emptied by capturing a hole or releasing its electron back to the conduction band. Recombination occurs when the center captures a free electron and holds it until emptied by capturing a hole. Thus, the recombination center may be considered a "stepping stone" in the gap between the bands. If the imperfection that creates the centers happens to be a foreign metal such as nickel or copper, the position of the center in the band gap would depend on the allowed energy level for the impurity in question. This is similar to the situation of the donor and acceptor impurities, except that the energy states for most metals are deeper in the band gap. The energy levels for some of the common metals of interest in silicon are given in

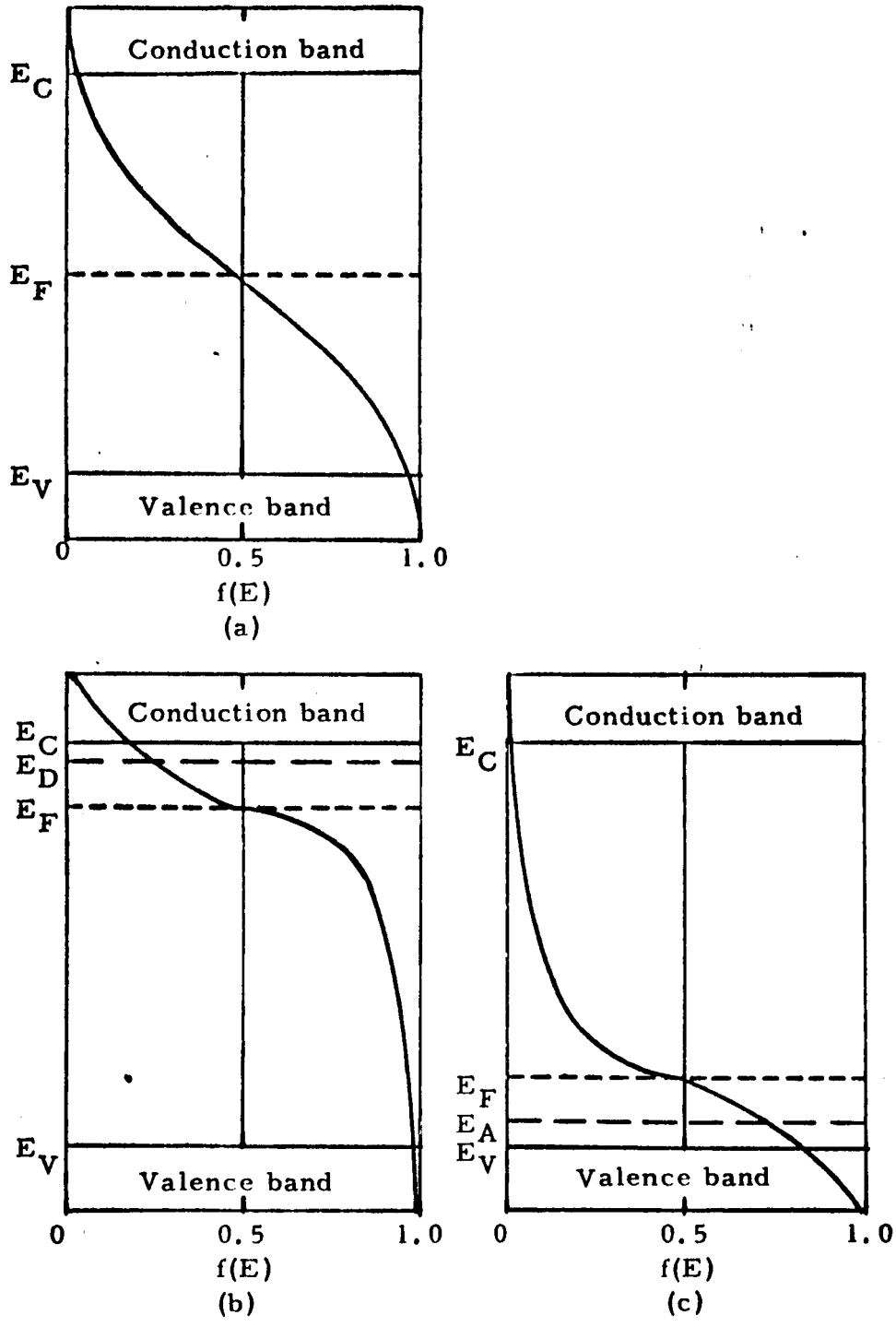

Fig. V. Positions of Fermi level for impurity semiconductors. (a) Intrinsic; (b) n type; (c) p type.

Fig. VI.[26]

It is apparent that several factors determine the probability of carrier recombination at a recombination center. They are[27] (1) the concentration of recombination centers in the crystal, (2) the concentration of the free carrier in question, which is related to resistivity, (3) the capture probability of the centers, and (4) the concentration of centers that are normally filled under equilibrium conditions. The last factor is dependent on the position of the centers in the band gap with respect to the Fermi level, since this would determine the degree of occupancy of the centers.

The beginning material for solid state radiation detectors is "p" type with boron as the acceptor impurity. Fig. V (c) corresponds qualitatively to the Fermi level for this crystal. It is obvious that the actual position of the Fermi level is dependent on the boron concentration. The activation energy of boron is 4.5×10^{-2} ev[28] establishing the acceptor energy level just above the valence band.

It has been established above that extrinsic conduction is the result of added impurities to an intrinsic silicon crystal. A larger concentration of an impurity causes more conduction states to be filled and enhances the conduction of the crystal. A graph showing resistivity as a function of acceptor and donor impurity concentration is shown in Figure VII.

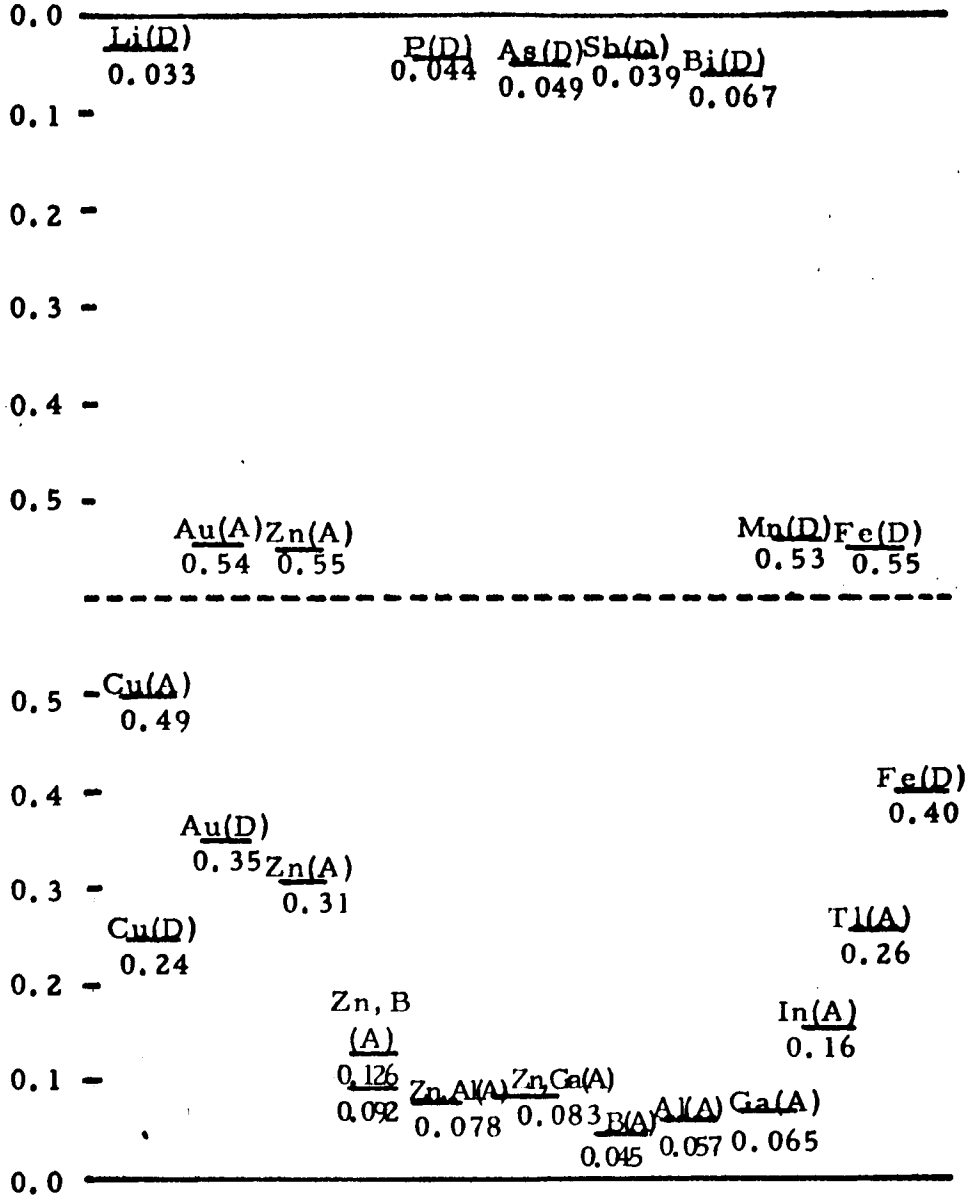

Fig. VI. Energy levels of impurities in silicon.

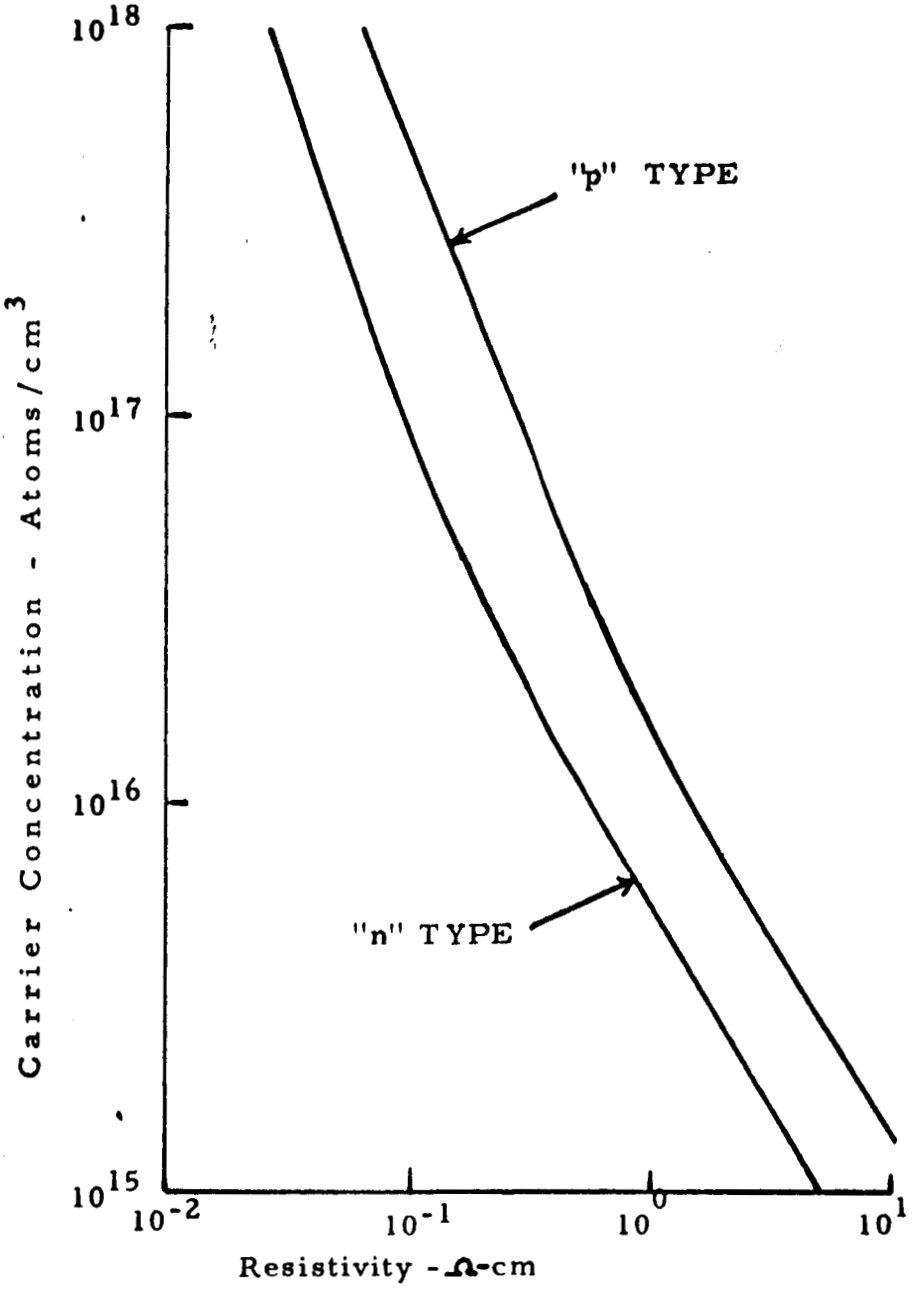

Fig. VII (a). Resistivity (10^{-2} - 10^{1} Ω-cm) as a function of carrier concentration in silicon.

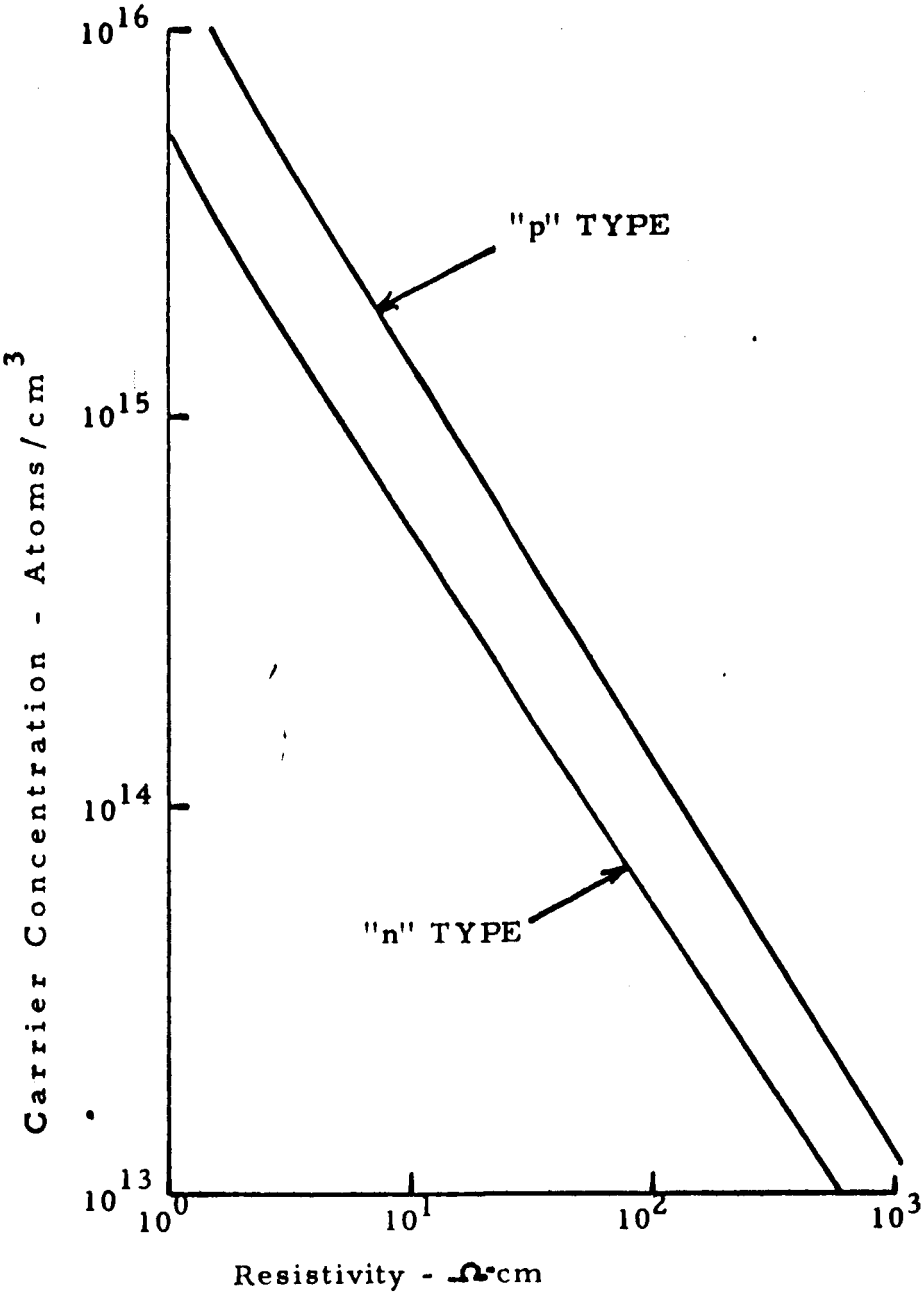

Fig. VII (b). Resistivity (10^0 - 10^3 Ω-cm) as a function of carrier concentration in silicon.

Obviously the movement of carriers is temperature dependent. A relationship can be derived beginning with the force equation

$$F = qE, \text{ and since } F = ma, \tag{26}$$

$$a = \frac{qE}{m}. \tag{27}$$

The average velocity of carriers through a crystal under the influence of an electric field is given by

$$V_D = a\,t, \text{ where } V_D \text{ is the drift velocity.} \tag{28}$$

Substituting (27) into (28) yields

$$V_D = \left(\frac{qt}{m}\right) E = \mu E \text{ cm/sec}, \tag{29}$$

where

$$\mu = \frac{qt}{m} \text{ is termed drift mobility.} \tag{30}$$

It is apparent that as the number of carrier collisions per unit time increases the drift mobility will decrease. The drift mobilities are influenced by the two principal collision mechanisms, (1) impurity-atom scattering and (2) lattice-vibration scattering. If μ_I is designated as the mobility due to impurities alone, and μ_L is lattice mobility, it is a fair approximation to write[29]

$$\frac{1}{\mu} = \frac{1}{\mu_I} + \frac{1}{\mu_L}. \tag{31}$$

The theory of impurity scattering mobility was investigated by Conwell and Weisskopf and their analysis gives the following formula:[30, 31]

$$\mu_I = \frac{8\sqrt{2}\,K^2\,(kT)^{3/2}}{\pi^{3/2} N_I\, q^3\, m_{eff}^{1/2}\, \ln\left(1 + \frac{3KkT^2}{q^2 N_1^{1/3}}\right)} \qquad (32)$$

where K = dielectric constant,

T = temperature ^{o}K,

N_I = total density of all ionized impurities,

m_{eff} = effective mass of electron or hole.

Actual measurements of drift mobility in high-quality crystals of silicon, where the impurity concentrations were so small that only lattice mobility would be predominant, give the following relationships for lattice mobility:[32]

$$\mu_{L_n} = 2.1 \times 10^9\, T^{-2.5} \qquad (33)$$

$$\mu_{L_p} = 2.3 \times 10^9\, T^{-2.7}$$

The composite effects of both impurity and lattice mobilities are shown in the curves of Fig. VIII.[33, 34, 35] These curves give the values of minority carrier drift mobility as a function of impurity concentration at room temperature for silicon. As is seen, the effect of impurity scattering becomes predominant at impurity

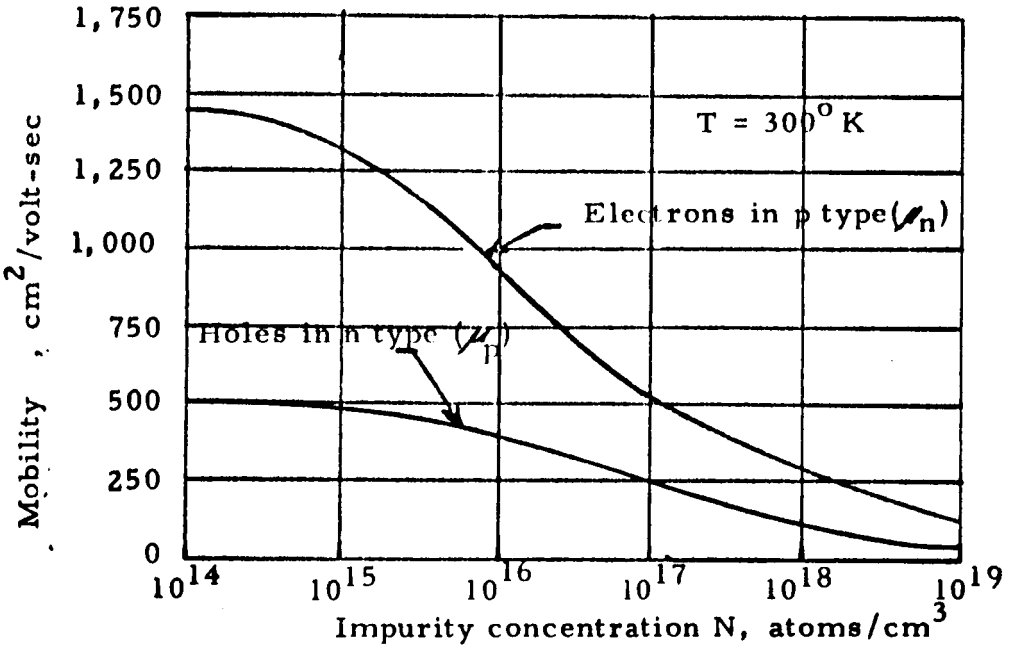

Fig. VIII. Drift mobilities in silicon.

concentrations of 10^{15} cm^{-3} or more. The mobilities have been reported by Dunlap[36] to vary as

$$\mu_n = 4.0 \times 10^9 \, T^{-2.6} \text{ cm}^2/\text{volt sec and} \qquad (34)$$

$$\mu_p = 2.5 \times 10^8 \, T^{-2.3} \text{ cm}^2/\text{volt sec} .$$

Pearson and Bardeen found a $T^{-3/2}$ law dependence of mobility upon temperature.[37] Regardless of which is correct, it is seen that the constant b defined as μ_n/μ_p approaches 3 in high resistivity silicon.[38]

Electric current is defined as the flow of a total amount of charge per unit time within an electric field. If a voltage is impressed on a semiconductor of length l and cross-sectional area A, the current density J for electrons would be

$$J_n = \frac{I_n}{A} = -qnV_{D_n} \quad \text{amps/cm}^2 . \qquad (35)$$

The current density for holes would likewise be

$$J_p = \frac{I_p}{A} = qpV_{D_p} \quad \text{amps/cm}^2 , \qquad (36)$$

where in (35) and (36) "n" and "p" are the electron and hole concentrations, respectively. Since the two in a crystal are additive,

$$J = J_n + J_p = -qnV_{D_n} + qpV_{D_p} . \qquad (36a)$$

Substituting (29) into (36a)

$$J = -qn(-\mu_n E) + qp\mu_p E. \tag{37}$$

$$J = Eq(\mu_n n + \mu_p p) \tag{38}$$

Setting $E = V/l$,

$$I = \frac{VA}{l} q(\mu_n n + \mu_p p). \tag{39}$$

Using Ohm's law,

$$R = \frac{V}{I} = \frac{l}{A} \frac{1}{q(\mu_n n + \mu_p p)} \tag{40}$$

Since this is the form of $R = \rho \frac{l}{A}$, where ρ is the resistivity,

$$\rho = \frac{1}{q(\mu_n n + \mu_p p)} \text{ ohm-cm}, \tag{41}$$

or, letting σ be the conductivity,

$$\sigma = \frac{1}{\rho} = q(\mu_n n + \mu_p p) \text{ mho-cm}^{-1}. \tag{42}$$

The curves in Figure VII show resistivity as a function of impurity concentration.

The treatment of semiconductor crystals would be partly incomplete without discussing the surface. It has been well established without adequate understanding that the electrical properties of a semiconductor surface differ from those of the bulk

interior. An abrupt boundary exists for the layer of surface atoms which will disrupt the orderly energy distribution in the region. Also the surfaces are never perfect. The atoms are very active in air and form oxide layers readily. Chemical ions, water atoms, and gas atoms, dependent on the ambient, may be absorbed by these layers. Considerable experimental work has shown this to be true. Also the surface exhibits a recombination rate for carriers which is usually different from the lifetime of the bulk material.

It is generally accepted from the early work of J. Bardeen, that at the surface there exist a number of surface energy states leaving energies that fall within the forbidden band gap of the semiconductor.[39,40] These states have been categorized into two types: (1) layer states and, (2) interface states. The layer states are generally believed to be due to the characteristics of the oxide layer arising from absorbed ions and are very sensitive to the ambient which the surface is exposed to. The interface states, as originally suggested by Brattain and Bardeen[41] act very similar to the recombination centers of the Shockley-Read-Hall theory.[42,43,44,45] These states are found to be independent of ambient, but dependent on the quality of the initial surface treatment by chemical etches before oxide formation. The number of layer states is usually greater than interface states.

Suppose the total ionic charge absorbed by the oxide layer on high resistivity "p" type material giving rise to layer states is positive. To maintain charge neutrality, electrons are attracted to the surface. This added concentration of electrons in the bulk region adjacent to the interface affects the Fermi level. It is customary to keep the Fermi energy as a constant reference and let the energy bands bend. Figure IX illustrates that the Fermi level is now closer to the conduction band, indicating that the conductivity of the surface reverses from "p" type to "n" type. The amount of the energy bands bend is a function of the density and energy distribution of the layer states, which is directly affected by the ambient. This conductivity reversal is called inversion and the layers thus formed are called inversion layers.

Since the density of interface states is smaller than that of the layer states, they do not appreciably affect inversion. However, the interface states have capture probabilities many orders of magnitude greater than the layer states.[46] Therefore, any observed recombination of carriers at the surface is attributed mainly to recombination at the interface centers. Surface recombination is expressed in terms of a surface recombination velocity, S, in centimeters per second. This is defined as the number of carriers recombining per second per unit area divided by the excess concentration over the equilibrium value at the surface.

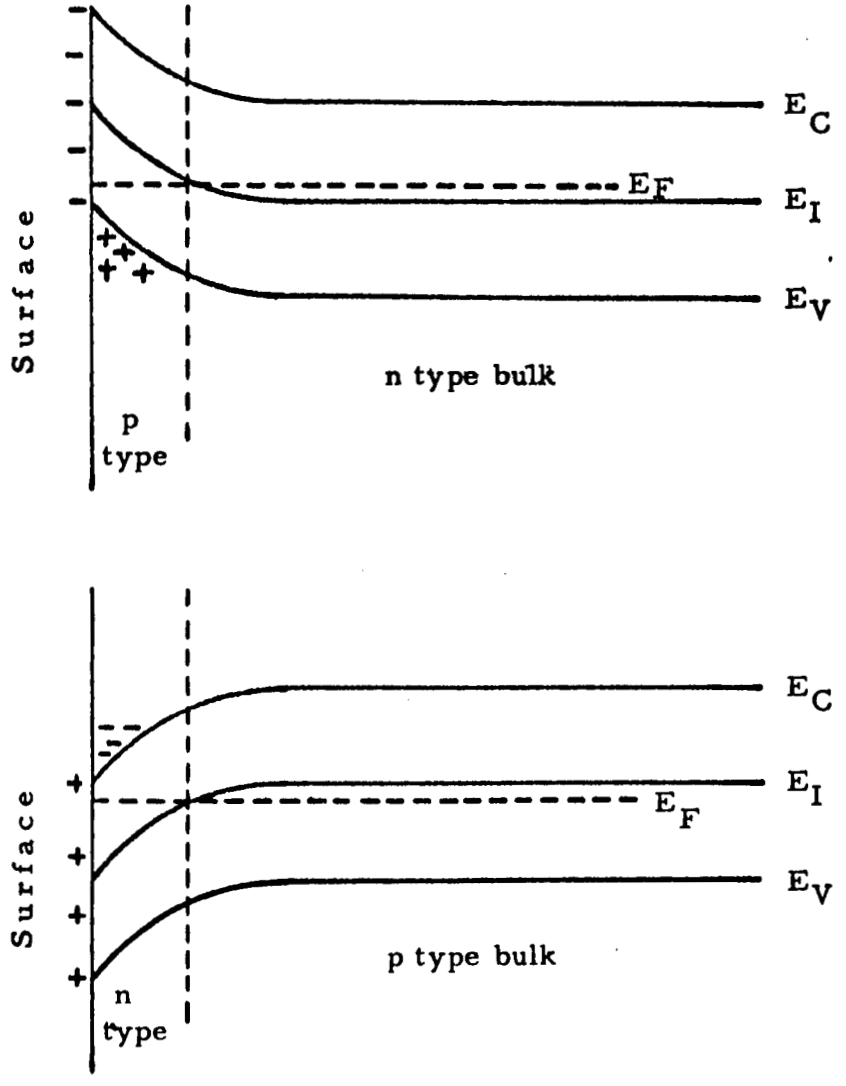

Fig. IX. Inversion layers in semiconductors.

It can be stated in conclusion that the density and energy levels of the interface states are determined by the method of initial surface treatment and are independent of any ambient effects. The ambient affects the nature of the ionic charge in the oxide layer states, which in turn alters the conductivity and type of the bulk layer just beneath the surface. Interface layers have the effect of lowering the effective crystal lifetime according to

$$\frac{1}{\tau_{eff}} = \frac{1}{\tau_{bulk}} + \frac{1}{\tau_{interface}} . \qquad (43)$$

Theory of Diffusions

In addition to motion by drift in an electric field, carriers may drift in a semiconductor crystal by diffusion in the absence of an electric field. This may be visualized by the consideration of an excess of holes or electrons in a localized region of a crystal at equilibrium. A spreading or diffusion in all directions would be observed. The rate of diffusion would be dependent on the concentration gradient. An analogy can be made to the flow of heat in a rod with a temperature gradient between the two ends. If an electric field is also applied, a drift motion is superimposed on the diffusion.[47]

For simplicity consider a one dimensional case of

diffusion.* Let the distribution of injected electron concentration be given by

$$n = n(x). \tag{44}$$

The concentration gradient is then $\frac{dn}{dx}$. It may, thus, be written

$$J_n = -c\frac{dn}{dx}, \tag{45}$$

where c is a constant. Consequently, c must include the electron charge -q. Therefore,

$$J_n = qD_n\frac{dn}{dx}, \tag{46}$$

where D_n is the diffusion constant for electrons in p-type material in cm^2/sec. Also,

$$J_p = -qD_p\frac{dp}{dx}. \tag{47}$$

Equations (46) and (47) form Fick's first law of diffusion,[48] or,

$$\vec{J} = -qD\vec{\nabla}n.$$

Substituting (46) and (47) into (36) yields

$$J = q\left(D_n\frac{dn}{dx} - D_p\frac{dp}{dx}\right). \tag{48}$$

---

*In a cubic lattice, such as silicon, symmetry requires an isotropic rate of diffusion making the diffusion rate a scalar. See, for instance, Kittel, Chapter I.

In three dimensions this becomes

$$\vec{J} = q(D_n \vec{\nabla} n - D_p \vec{\nabla} p) . \tag{49}$$

The diffusion constants are related to the mobility by the Einstein relationship[49]

$$D = \mu \frac{kT}{q} \text{ cm}^2/\text{sec} , \tag{50}$$

where

k = Boltzmann's constant,

T = absolute temperature.

An important property of carriers, related to lifetime,* is diffusion length which is defined by the equation[50]

$$L = \sqrt{D\tau} \tag{51}$$

where τ is the carrier lifetime. When a small density of carriers is injected into a semiconductor, the density will decrease proportionally as $e^{\frac{-t}{\tau}}$. When $t = \tau$, the density has decreased to 1/e of the original value. Therefore, the lifetime τ is a measure of the recombination rate. Shockley[51] showed that lifetime due to

---

*The lifetime of a carrier is the average time between generation and recombination. It should not be confused with the mean free time associated with mobilities, since a carrier may experience many collisions before it recombines.

carrier concentrations only is given by

$$\tau_c = \frac{n_i^2}{e(p+n)} , \qquad (52)$$

where e is the rate of thermal emission of carriers. The effect of the recombination centers on the carrier lifetimes is given by the Shockley-Read-Hall[42,43,44,45] theory based on probability considerations employing Fermi-Dirac statistics. By their analysis it was shown that lifetime depends inversely on the recombination center concentration. Substituting Equation (50) into (51) yields

$$L^2 = \frac{kT\mu}{q} \tau . \qquad (53)$$

By comparing Equation (53) with the published values for mobility, it is seen that the diffusion length varies inversely with temperature.

The diffusion coefficient varies with temperature as[52]

$$D = D_o e^{-\frac{\Delta E_a}{kT}} , \qquad (54)$$

where

ΔE_a = energy of activation

D_o = apparent value of D at infinite temperature.

The diffusion coefficient determined experimentally for lithium in "p" type silicon[53,54,55] is

$$D = 2.30 \times 10^{-3} \exp\left(-\frac{0.72 \text{ ev}}{kT}\right) \text{cm}^2/\text{sec} \qquad (55)$$

for a temperature range of 0°C to 877°C. A curve showing D as a function of T is shown in Fig. X.[56]

The process of diffusion of holes and electrons is described by the differential equations (one-dimensional case)

$$D_p \frac{\partial^2 p}{\partial x^2} = \frac{\partial p}{\partial t} \qquad (56)$$

and

$$D_n \frac{\partial^2 n}{\partial x^2} = \frac{\partial n}{\partial t} \qquad (57)$$

assuming the diffusion coefficient not to be a function of concentration. Equations (56) and (57) form Fick's second law of diffusions.

If an "n" type dopant such as lithium, which dopes interstitually, is deposited on the surface of "p" type material such that the source may be considered infinite or constant, the solution to equation (57) is[57]

$$N(x) = N_o \operatorname{erfc}(x / 2\sqrt{Dt})$$

where

N_o = surface concentration

$N(x)$ = concentration at a depth x

t = time

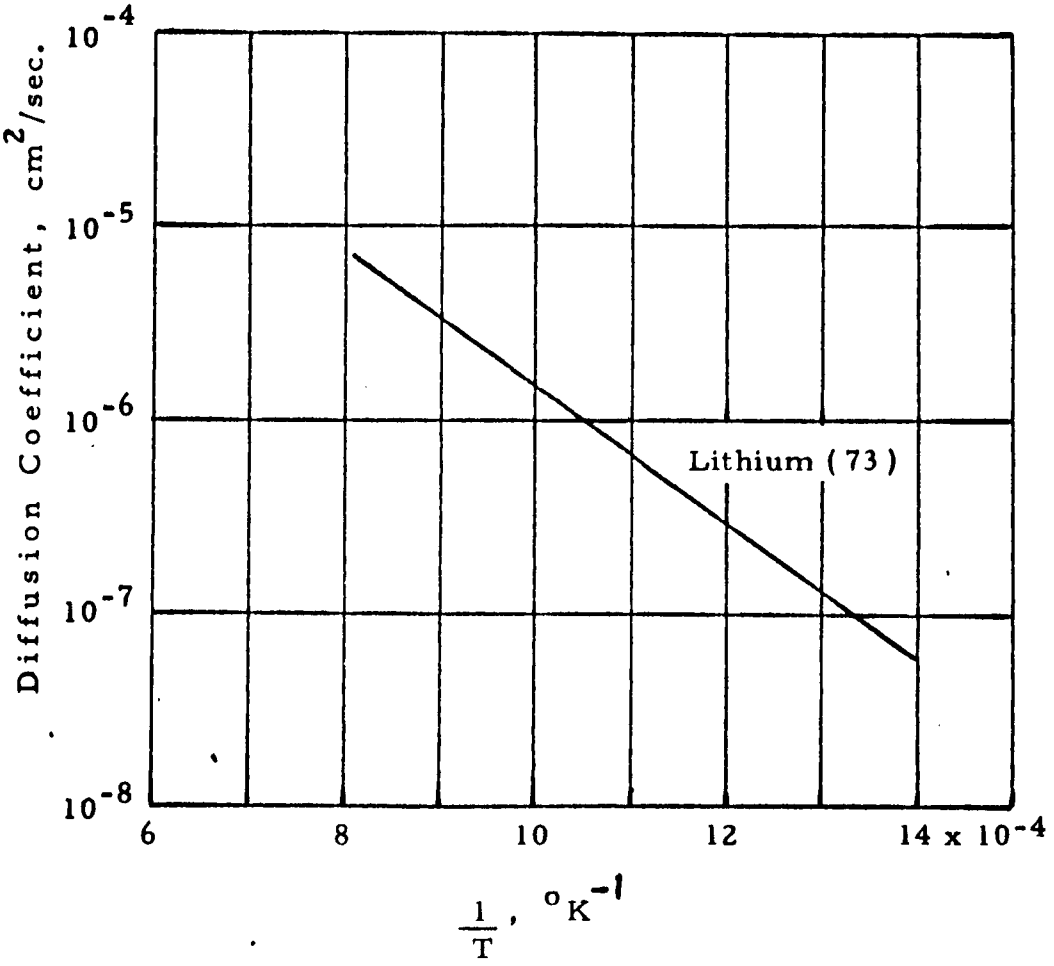

Fig. X. Diffusion coefficient of lithium in silicon as a function of temperature

and

$$\operatorname{erfc} u \equiv \frac{2}{\sqrt{\pi}} \int_u^{\infty} e^{-y^2}\, dy.$$

Theory of "P-N" Junctions

Assuming the donor concentration N_D is greater than the acceptor concentration N_A ($N_D > N_A$), there will be two regions with different type conduction. Thus, a "p-n" junction is formed.[58] A typical impurity profile and energy diagram[59] for a graded junction are shown in Fig. XI.

At the transition region the holes in the "p" region will diffuse, because of the impurity gradient, across the junction into the "n" region where the hole concentration is small. Likewise, electrons from the "n" region will diffuse into the "p" region where the electron concentration is small. Since the impurity ions are fixed in the lattice and are not free to move, as a result of the diffusion, there will be regions of unneutralized charge on both sides of the junction. Since the bare charge on each side of the junction is opposite in polarity an electric field is established which, at equilibrium, prevents majority carrier diffusion. The depleted layer is very similar to a parallel plate capacitor and will have a capacitance.

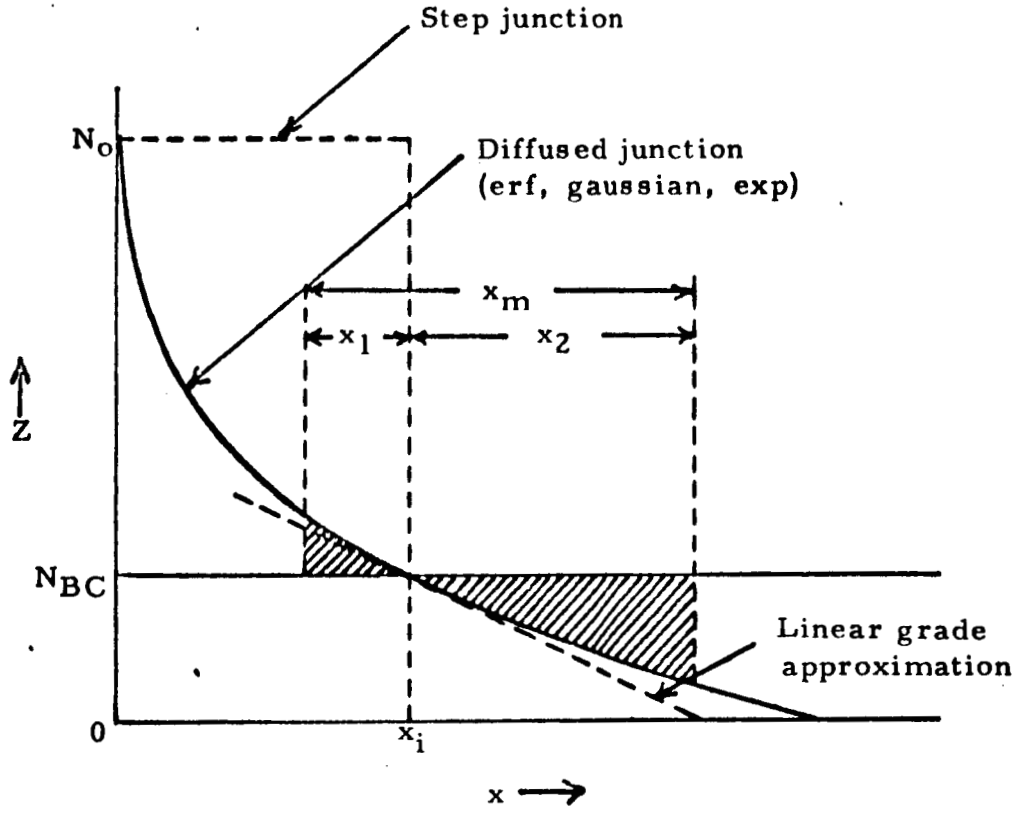

Fig. XI (a). Impurity profile and depletion-layer characteristics for diffused junctions.

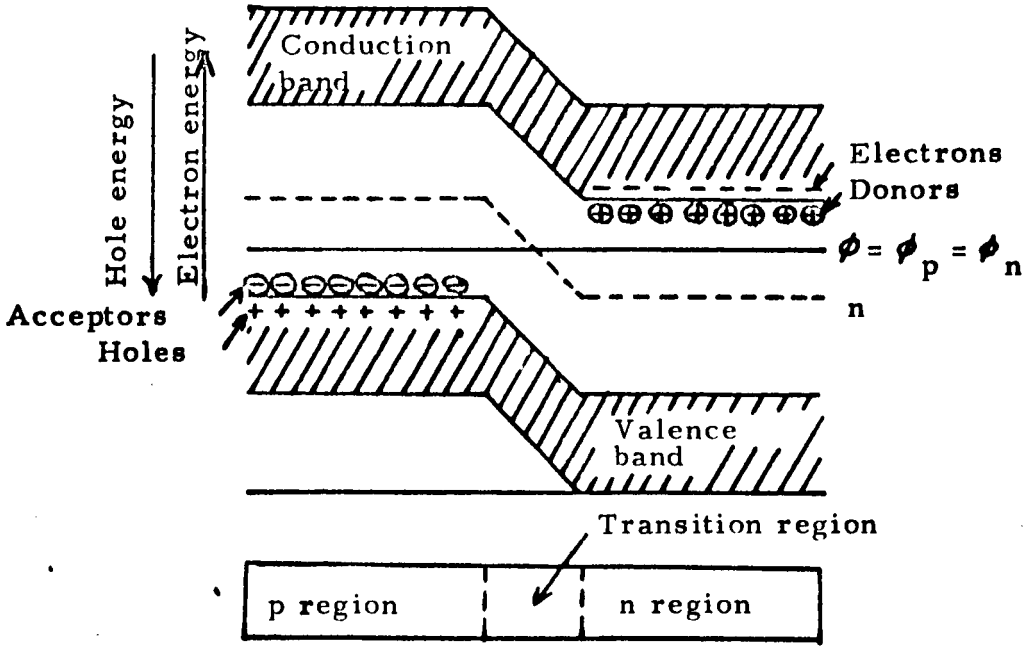

Fig. XI(b). Energy diagram for a p-n junction in equilibrium illustrating constant Fermi level.

If a supporting electric field, reverse bias, is applied to this "n-p" junction the depletion layer will widen. In the reverse biased condition there will be a small reverse current due to the minority carriers within one diffusion length of the junction that will diffuse to the transition region and drift across because of the electric field. This current remains fairly constant with an increase in voltage until the carriers acquire sufficient energy to break additional valence bonds upon collision.[60] This results in further generation of electron-hole pairs, causing the reverse current to multiply. If this voltage is increased slightly, the process becomes so cumulative that an avalanche occurs and the junction "breaks down" completely.[61]

An opposing field, forward bias, will cause the depletion layer to become narrow until the internal field is exceeded. There is then no potential "barrier" and a further increase in voltage causes a large flow of current.

Junctions formed by diffusion methods are graded since the diffused region establishes a gradual transition from one impurity type to the other. In the depletion region it is a good approximation to assume the grade to be linear. Therefore,

$$N(x) = ax \tag{59}$$

where a is the grade constant in atoms/cm^4. Because of the linear

grade of the impurities, the net charge density will also be a linear function, or

$$\rho(x) = qax. \tag{60}$$

For a distance x on either side of x = 0, the areas are equal, which indicates that the depletion spreads equally in both directions. The total depletion is then x_m. From Poisson's equation,

$$\frac{d^2V}{dx^2} = -\frac{\rho(x)}{k\epsilon_o}, \tag{61}$$

it is shown in the appendix that

$$x_m = \left(\frac{12k\epsilon_o V}{qa}\right)^{1/3} \text{ cm} \tag{62}$$

and

$$C_T = \left(\frac{(k\epsilon_o)^2 qa}{12V}\right)^{1/3} \text{ farads/cm}^2. \tag{63}$$

Similar calculations for a step junction where

$$\rho(x) = -qN \tag{64}$$

results in

$$x_m = \left(\frac{2k\epsilon_o V}{qN_A}\right)^{1/2} \text{ cm for "p" type} \tag{65}$$

and

$$C_T = \left(\frac{q k \epsilon_o N_A}{2 V}\right)^{1/2} \text{ farads/cm}^2 \text{ for "p" type.} \quad (66)$$

k for silicon is 12. Actual experimental measurements of capacitance indicate that diffused junctions do exhibit a $V^{-1/3}$ dependence at low voltages.[62] At higher voltages, the dependency becomes $V^{-1/2}$.[63] Extensive study of capacitance calculations have been made by Lawrence and Warner.[64]

Theory of Drift

As previously stated lithium diffuses interstitually. When held at an elevated temperature, the probability of a lithium atom migrating through a silicon crystal becomes higher. If an electric field is superimposed on this system, the lithium ions will drift in the direction of the electric field and effect a very high degree of boron ion compensation in the depletion region.[65] provided that the temperature is not high enough for the intrinsic "n" concentration to cause flooding.* As a result of this compensation, the depletion region must spread more into the "p" region. Assuming sufficient lithium, this process will continue during the length of voltage

*Flooding is the term describing the condition of thermally generated carriers being equal to or greater than the diffused carriers.

and temperature application. The width of the compensated region is given by[66]

$$W = (2\mu V)^{1/2} t^{1/2} \qquad (67)$$

where $2\mu V$ is defined as the drift parameter and t is time. A lithium drift parameter nomograph for oxygen-free silicon and a family of curves for drift depth as a function of time for various drift parameters are given by Blankenship and Barkowski.[67]

The minimum surface concentration of lithium atoms needed to compensate the drifted region is given by[68]

$$N_S (\text{atoms/cm}^2) = N_H \cdot W \qquad (68)$$

where N_H is the hole concentration in the starting silicon.

Theory of Operation

When a reverse bias is applied to a compensated diode, the depletion layer spreads very rapidly through the compensated region to make it intrinsic. The resulting device is "N-I-P" in structure. Any form of radiation incident on the device will form electron-hole pairs in the silicon by absorbing 3.6 ev[69] of energy per electron-hole pair. The carriers in the intrinsic region will be swept away by the electric field. This movement of charge constitutes an electric current which when passed through the circuit shown in Figure XII

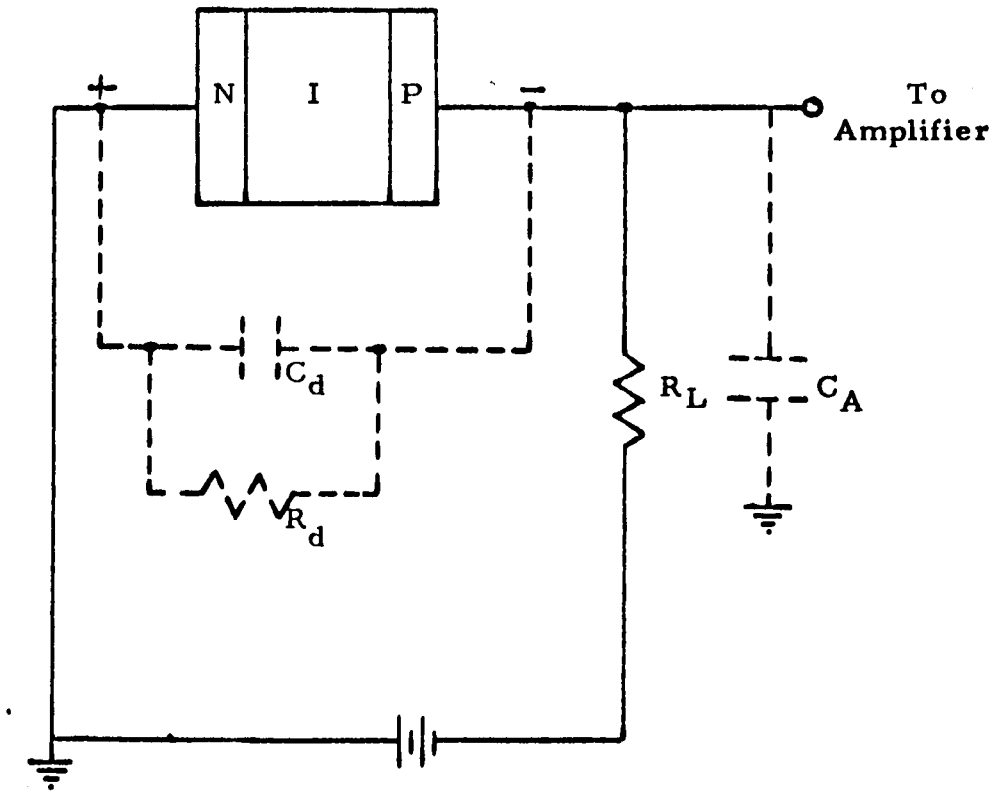

Fig. XII. Applicable circuit for nuclear particle detector.

develops a voltage pulse. Appropriate analysis of this amplified pulse gives a measure of the incident radiation energy.

In the absence of radiation, there will be a small "reverse current" under reverse biased conditions. This current has three components:[70]

(1) The drift current due to diffusion of minority carriers into the depletion region;

(2) The carrier generation current, due to carriers produced by thermal generation in the depletion region;

(3) The surface leakage.

In practice the former two components are usually negligible compared with the surface leakage. This leakage current is a source of diode noise[71] and is the predominant noise generator. Causes of this charge flow include ionic charges on the surface, conducting films on the detector, conducting ambients and inversion layers across the diode surface.

Extensive studies[72] made of electrical noise in semiconductor devices show that there are three types:

(1) Thermal noise, often called Johnson noise, due to fluctuations in the spatial distribution of carriers arising from thermal diffusion;

(2) Current noise, often called shot noise, due to statistical fluctuations in the number of carriers leading to changes in conductivity;

(3) Flicker noise, often called 1/f noise, believed to originate at the surface and is dependent on surface leakage and contact resistance.

Good detector performance demands that the noise to signal ratio be low so that the resolution is not limited.

PREPARATION OF DETECTOR

The beginning material selected was Lopex* "p" type boron doped silicon with the following specifications:

Lifetime	>	100 μsec
Dislocation density	<	$3,000/cm^2$
Oxygen concentration	<	10^{15} atoms/cm^3
Resistivity		300-500 Ω cm

Lopex material, rather than melt grown or float zone, was chosen because it offers the advantages of low oxygen concentration and dislocation density. Melt grown silicon has extremely low dislocation density but high oxygen content. Float zone material has very low oxygen content but high dislocation density.

A minimum lifetime specification was imposed to insure the highest possible carrier mobility. As discussed in the theory section, this is extremely important for good charge collection properties of the resulting detector. In an implicit manner this limit also imposes a heavy metal concentration maximum. This is because the metals would effect a high recombination probability and, thus, limit the lifetime.

---

*Lopex is Texas Instrument's tradename for specially processed silicon crystals to achieve extremely low, less than 10^{15} atoms/cm^3, oxygen content and low dislocation density.

The maximum dislocation density was specified to lessen the number of spikes* during diffusion, to lower the resulting device noise, and to increase the lifetime. This limit may have been quite unnecessary with the chosen material. However, some process abnormality may have existed during its growth causing a flaw in the material. Without this specification the flaw may not be detected.

From elementary chemistry it is known that lithium and oxygen react with extreme ease to form lithium oxide. This was the primary reason for specifying a maximum oxygen content in the silicon crystal. The reaction could have caused very poor compensation during the following drift process. It is also widely known that oxygen has a very unpredictable effect on the crystal resistivity during heat treatments. One hundred per cent changes in resistivity are not uncommon when a high concentration of oxygen is present.

The 300-500 Ωcm resistivity range was a compromise between the resulting diode avalanche breakdown and leakage. It was shown in the theory section that the "np" product is a constant for a given temperature. Also, the diode leakage is dependent on the

---

*A spike is caused by an impurity diffusing in a localized area with a much higher diffusion coefficient than in the rest of the material. This causes a much deeper penetration in this area than elsewhere. Junctions of this nature usually exhibit extremely low avalanche breakdowns.

minority carrier concentration. Lower resistivity "p" type material would have lower "n" type concentration and, consequently, lower diode leakage. This was desirable since detector noise is caused by the leakage current. However, it was also desirable to have the avalanche breakdown high enough to allow 1500 volt operation of the prepared detector. The chosen resistivity allows the realization of both of these parameters.

13 cm x 2 cm x 1 cm slabs were sawed from the grown crystals. The 13 cm length was necessary to stop 200 Mev protons. The 2 cm width and 1 cm thickness were helpful in achieving a 1 cm^2 cross sectional area.

After sawing, the slabs were cleaned by ultrasonic vibration in trichloroethylene. The vibration freed loose impurity particles lodged in the silicon surface during the sawing operation. Organic compounds on the surface were partially dissolved by the trichloroethylene. This type cleaning process is considered an excellent one by the semiconductor industry. Its use removes many particles not removable by any other known method. From this point extreme caution was exercised to not expose the bars to a contaminated atmosphere.

Many detector fabricators etch the silicon at this point in Bell 39A* or some similar etch to polish the surface. This process

---

*Bell 39A is a silicon etch developed by Bell Laboratories consisting of hydrofluoric, nitric, and acetic acid.

is advantageous if the lithium in the following diffusion step is deposited from a vapor state or is evaporated onto the surface. With the type lithium deposition used in this work, difficulty was encountered in achieving uniform impurity concentrations with polished surfaces. In order that the above etching step could be eliminated, the most elaborate cleaning techniques known had to be used.

The slabs were immersed in 150° C concentrated sulfuric acid for fifteen minutes to oxidize and remove any organics remaining on the surface. If the acid became discolored, this step was repeated. This operation is presently suspected of inducing "strange" surface states in the silicon. No conclusive literature has yet been published on this subject. A fifteen-minute immersion in 150° C nitric acid was then employed to dissolve any heavy metals remaining on the surface. As before, this step was repeated if the acid became discolored. Two fifteen-minute deionized water boils followed to remove the ions remaining from the acid cleans.

Lithium diffusion followed immediately before the slices could be contaminated with impurities that would diffuse into the silicon. Three parts of a viscous solution of five parts piecin wax, three parts bees wax and benzene were mixed with five parts of a lithium in oil suspension. The thick crust of lithium formed by letting a lithium in oil suspension sit overnight was used for the five parts lithium. The paste thus formed was spread on the slab

surfaces by continuous circular motion of some clean wooden applicator. A larger area than the desired junction area was coated. It was very necessary that the surface be thoroughly wetted with the paste. Lithium was then diffused into the silicon for five minutes in a dry nitrogen atmosphere on a hot plate previously stabilized at 400° C. A nitrogen atmosphere, or any inert one, was necessary to prevent oxidation of the lithium. The slabs were then slow cooled, also in a dry nitrogen atmosphere, on a piece of quartz. This helped to increase the carrier lifetime in the bulk silicon.

Removal of the resulting lithium crust was accomplished by immersing the slab in benzene. Trichloroethylene swabbing was then used to thoroughly clean the surface. A ten-second etch in a three parts nitric to one part hydrofluoric acid solution was employed to remove part of the damaged surface. This damage was caused by the lithium alloying into the silicon. It was possible to determine the quality of the diffusion by the uniformity of this damage. If it was felt that a poor diffusion, more accurately determined by a four point probe, was achieved, the slab was lapped with 1800 abrasive to remove the lithium and reprocessed.

A viscous solution of five parts piecin wax and three parts bees wax dissolved in benzene was used to mask an area of the lithium diffused face 1.5 cm wide and 13 cm long. This masking process was performed under a heat lamp to boil off the benzene and

make the acid resistant coating adhere to the surface better. Much care was taken to mask an area inside the preceeding lithium diffused area. The unprotected sides and face were etched twice for two minute intervals in a clean solution of three parts nitric and one part hydrofluoric acid. The slabs were quenched in clean room temperature deionized water or dilute nitric acid to prevent staining. Boiling trichloroethylene was used to remove the wax coating. Two fifteen minute clean deionized water boils followed immediately to remove the remaining acid ions.

By this manner, a mesa was formed which produces a clean well defined "n-p" junction. It was necessary to have a large enough volume of etch to prevent overheating of the solution. The etch rate was dependent on the etch temperature. Consequently, if the solution became hotter, the etching would progress at a much higher rate. Utmost caution was exercised to protect this exposed junction from any impurities that would cause junction leakage during the following drift process.

At this point the junction leakage was measured while reverse biased with 300 volts. All reverse currents were less than 10 micro amperes. This current was indicative of the junction quality.

Approximately 100 angstroms of pure aluminum were evaporated onto the back side and a 1.0 cm x 11.0 cm stripe inside the topside junction area of the slab to give good ohmic contact during

the drift procedure. No aluminum was allowed to overlap onto the sides and across the "n-p" junction to form a leakage path.

The drift procedure was performed on a hot plate previously stabilized at 135° C in an air atmosphere. A reverse bias of 400 volts was maintained with the current limited to 100 milliamperes with a constant current power supply. An aluminum chamber was used in an attempt to attain a constant temperature. It was necessary to stop the drift once, when the leakage current became excessive, and reetch the mesa. The increased current was caused by surface inversion when the silicon oxidized. Much literature has been published showing that the segregation coefficient of boron in silicon and silicon dioxide favors silicon dioxide. Thus, as silicon dioxide was grown, the boron was depleted from the silicon surface. Since very high resistivity material, low boron concentration, was used the surface inverted to "n" type very easily. This resulted in a thin conducting layer on the surface for leakage current to flow. A short etch removed this layer and again extended the "n-p" junction to the surface. Many detector fabricators drift in a silicone oil bath to prevent the growth of silicon dioxide and to produce a constant temperature. This is a much better process than the one used here. However, expensive equipment is necessary which could not be justified for small volumes. By using the precautions mentioned above excellent detectors of various geometries were produced.

Using the nomograph of Blankenship and Barkowski, a drift parameter ($2\mu V$) of 6×10^{-7} cm^2/sec was determined for V = 400 V and T = 135° C. The calculated time, by equation (67), for a 4 mm. drift depth was seventy-four hours. It was verified by earlier work where full slice drift was performed that the equations derived by Blankenship and Barkowski were extremely accurate. Consequently, the drift was allowed to proceed for forty-eight hours, at the above conditions and ninety hours at 250 V and 130° C. This was the nearest convenient time to the one calculated.

Again, the mesa was masked and the sides and aluminum back were etched for two two-minute intervals in clean etch solutions. Two clean water rinses followed before the wax was removed by boiling trichloroethylene and swabbing. The slabs were then cleaned with two fifteen-minute water boils and dried with methyl alcohol. Since this was the final cleaning process, every possible precaution was exercised to keep from introducing any impurities.

The detector was then passivated by coating all of the silicon except a 0.5 cm wide strip on the "n" and "p" faces with Dow Corning 1440 varnish. Care was taken to thickly and evenly coat the surfaces immediately after the final clean to achieve the best possible passivation. A twenty-four hour curing followed in a dry dust free atmosphere at 25° C. Its purpose was to allow the varnish to dry with very little ionic contamination.

A conducting epoxy* was used to mount the completed detector on a 1 cm x 12 cm brass strip. A thin layer of the epoxy was spread over the entire "p" face and placed down flat on the strip. This also formed contact to the "p" material. The 0.5 cm wide opening on the lithium face was then coated with the epoxy. One end of a 10 cm length of 8 mil copper wire was inserted in the coating. The whole system was allowed to dry for twenty-four hours. After this period the brass strip was mounted on the top, ground side, of a B&C connector. The copper wire was connected to the positive terminal with conducting epoxy. A twenty-four hour drying cycle followed before the detector assembly was handled. Figure XIII shows a photograph of the finished assembled detector.

*E-Soldier 3021 Silver Epoxy manufactured by: Epoxy Products, Inc., of Irvinton, New Jersey, was used.

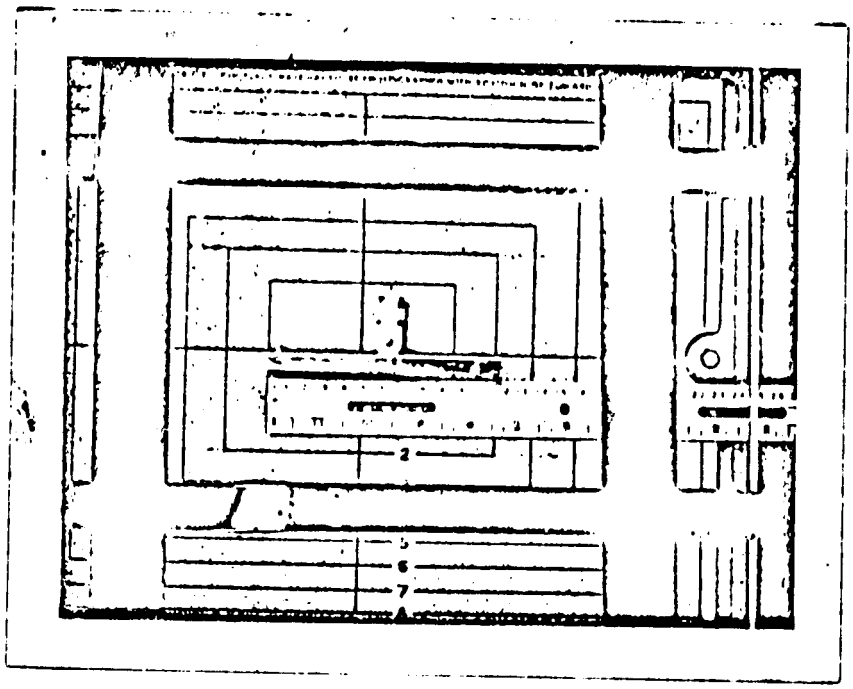

Fig. XIII., Photograph of Assembled detector.

EXPERIMENTAL RESULTS

The reverse bias leakage current measured at 300 volts was 8 micro amperes. A depletion layer width of 5.8 mm was calculated. Figure XIV shows a plot of the device capacitance as a function of voltage. Capacitance measurements could not be made beyond 600 volts. However, it appears that the capacitance approaches 90 pico farads at very high voltages.

The detector was used to measure the energy absorbed by various thicknesses of silicon bombarded with 159.75 Mev protons. A bias of 1500 volts was used to achieve full charge collection. Following is a list of the system equipment used in conjunction with the detector:

1. Tennelec Model 90 power supply,
2. Tennelec Model 1008 preamplifier,
3. Hewlett Packard Model 120B oscilloscope,
4. Textronix Type 317 oscilloscope,
5. RIDL Model 47-7 pulse generator,
6. RIDL Model 23-3 display readout,
7. RIDL Model 24-1 Thin Film memory channel analyzer.

A block diagram is shown in Figure XV.

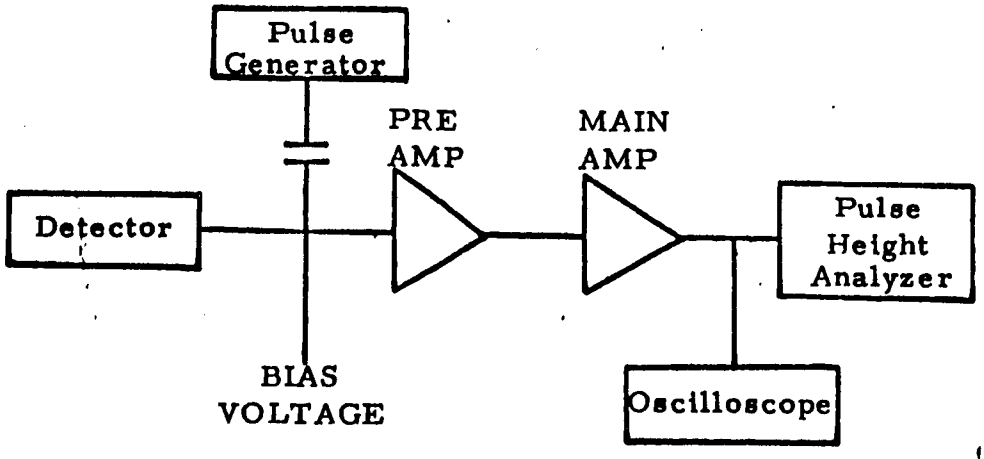

FIG. XV. BLOCK DIAGRAM OF PULSE ANALYZING EQUIPMENT

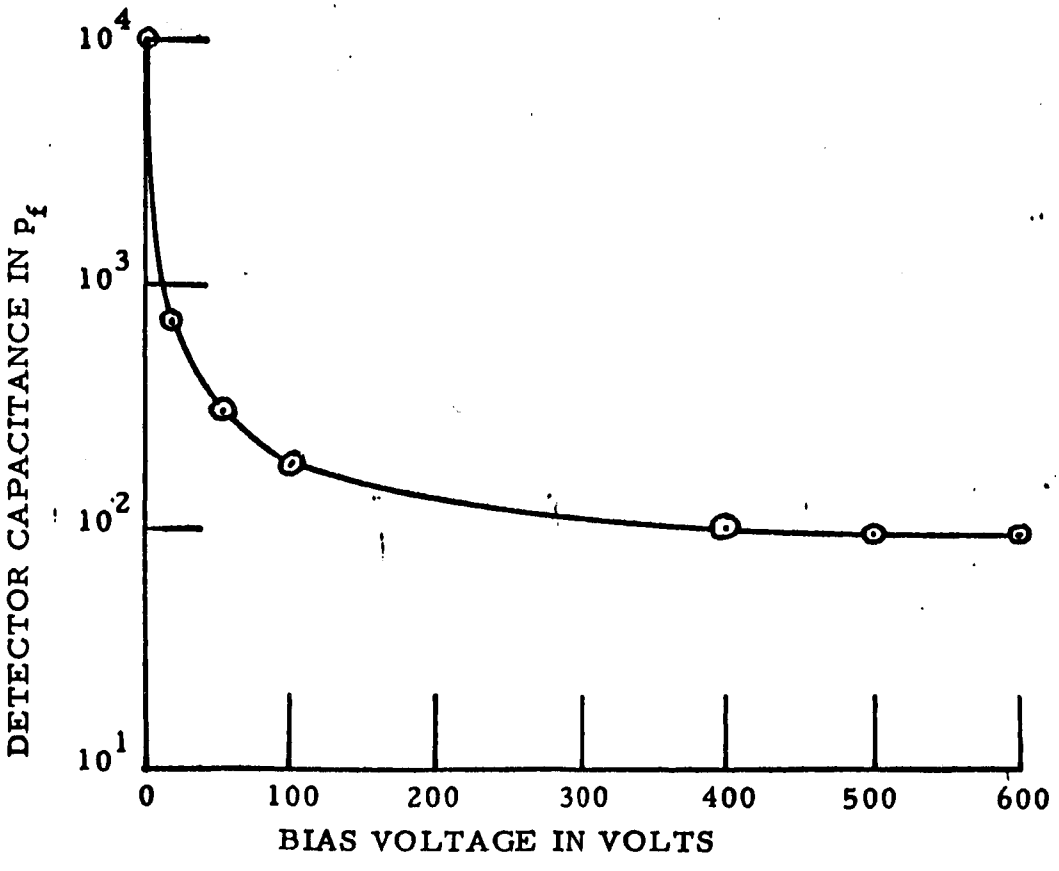

FIG. XIV. DETECTOR CAPACITANCE AS A FUNCTION OF VOLTAGE

With the pulse generator, an 80.49 system amplification was determined and the voltage per channel 0.02045. While biased at 1500 volts, the protons were passed through a silicon absorber and into the end of the detector parallel to the depletion region. The detector voltage pulse was amplified and stored in the channel analyzer according to its amplitude. An oscilloscope was used to observe the amplified pulses. The signal to noise ratio was approximately 40:1. Pulses of this nature were counted until the sample (approximately 1000) was valid statistically. This plot was recorded on an automatic typewriter. Proton energy was measured after passing through approximately 10, 15, 20, 25, and 30 Mev absorbers. A most probable channel to the nearest one hundredth was determined with the aid of a computor for each distribution. Table 1 lists the most probable channel, the shift in channel number, the energy loss, the incident energy, and ρdx of the silicon absorber. The energy loss is calculated by multiplying ΔV by 0.49055 Mev/channel, the previously determined energy per channel.

According to the Bethe-Block equation[73] the stopping power of an absorber is given by

$$S = -\frac{dE}{\rho dx} = \frac{4\pi mc^2 r_o^2 N_o}{\beta^2} \frac{Z}{A} \left[\ln \frac{2mc^2 \beta^2}{1-\beta^2} - \beta^2 - \ln 1 - \frac{\sum C_i}{Z} \right] \quad (69)$$

in Mev cm^2/gm.

TABLE 1

DATA ON PROTON ENERGY AFTER VARIOUS ABSORPTION

Most Probable Channel	ΔV	ΔE	E_{ai} Mev	ρdx Gm/cm^2
322.60	0	0	159.75	0
302.22	20.28	9.996	149.75	2.3287
291.64	30.86	15.187	144.56	3.5033
280.77	41.73	20.520	139.23	4.6556
269.50	53.00	26.048	133.70	5.8195
257.88	64.62	31.748	128.00	6.9831

ρ = density of absorber

Z = Atomic number of absorbing material

A = Atomic weight of absorbing material in gms.

β = v/c, velocity of the incident particle relative to the velocity of light.

C_i / Z = Shell corrections of the i-th shell.

I = Average excitation potential per electron of the stopping atom. I, by definition, is a constant.

Letting $F_2(\beta) = \dfrac{4\pi mc^2 r_o^2 N_o}{\beta^2}$

$$F_1(\beta) = \ln \frac{2mc^2\beta^2}{1-\beta^2} - \beta^2 ,$$

and $$\ln I' = \ln I + \frac{\sum C_i}{Z}$$

$$S_a = F_2(\beta_a) \frac{Z}{A} F_1(\beta_a) - \ln I_a' \qquad (70)$$

The measured stopping power, $\frac{dE}{\rho dx}$, may be defined as

$$\frac{E_1 - E_2}{\rho dx} = \frac{\Delta E}{\rho dx} = \frac{S_1 + S_2}{2} \qquad (71)$$

where S_1 is the stopping power at the initial energy, E_1, the proton has as it enters the absorber, ρdx, and S_2 is the stopping power at the emergent energy of the proton. Thus, a system of equations can be written for 2, 3, or 4 absorbers.

$${}_1T_2 = \frac{E_1 - E_2}{\rho \Delta x_a} = \frac{S_1 + S_2}{2} \qquad (72)$$

$${}_1T_3 = \frac{E_1 - E_3}{\rho \Delta x_b} = \frac{S_1 + S_3}{2} \qquad (73)$$

$${}_2T_3 = \frac{E_2 - E_3}{\rho(\Delta x_a - \Delta x_b)} = \frac{S_2 + S_3}{2} \qquad (74)$$

Solving as a set of 3 equations with 3 unknowns,

$$S_1 + S_2 = 2_1T_2 \text{ and} \tag{75}$$

$$S_1 + S_3 = 2_1T_3 . \tag{76}$$

Adding (75) and (76) yields

$$2S_1 + S_2 + S_3 = 2({}_1T_2 + {}_1T_3). \tag{77}$$

Also,

$$S_2 + S_3 = 2_2T_3. \tag{78}$$

Subtracting (77) from (78) yields

$$2S_1 = 2({}_1T_2 + {}_1T_3 - {}_2T_3). \tag{79}$$

$$S_1 = {}_1T_2 + {}_1T_3 - {}_2T_3 \tag{80}$$

Solving (75) for S_2 gives

$$S_2 = 2_1T_2 - S_1. \tag{81}$$

Similarly,

$$S_3 = 2_1T_3 - S_1, \tag{82}$$

$$S_4 = 2_1T_4 - S_1, \tag{83}$$

$$S_5 = {}_2T_5 - S_1, \tag{84}$$

$$S_6 = {}_2T_6 - S_1. \tag{85}$$

We now have values of the stopping power at specific proton energies. Since E is known, β_a, $F_1(\beta_a)$ and $F_2(\beta_a)$ can be calculated.

There was an energy uncertainty of 0.005 Mev and a ρdx uncertainty of 0.001 gm/cm^2. Consequently, only a range can be determined for the stopping powers. Table II shows the maximum, most probable and minimum values calculated by equations (80) through (85). A sample calculation is as follows:

Channel number for E_1 is 322.60.

Channel number for E_2 is 302.22.

Then ΔV is 20.38.

20.38 x 0.49055 Mev/channel gives ΔE = 9.996 Mev.

$${}_1T_2 = \frac{\Delta E}{\rho dx} = \frac{9.996}{2.3287} = 4.2925$$

Channel number for E_3 is 291.64; ΔV = 30.96.

30.96 x 0.49055 Mev/channel = ΔE = 15.187

$${}_1T_3 = \frac{\Delta E}{\rho dx} = \frac{15.187}{3.5033} = 4.3351$$

$${}_2T_3 = \frac{\Delta_2 E_3}{\rho \Delta_2 x_3} = \frac{15.187 - 9.996}{3.5033 - 2.3287} = 4.4185$$

$$S_1 = {}_1T_2 + {}_1T_3 - {}_2T_3 = 4.2925 + 4.3351 - 4.4185$$

$S_1 = 4.2091$

$S_2 = 2_1T_2 - S_1 = 2 \times 4.2925 - 4.2091 = 4.3759$

These experimentally determined values of stopping power and the calculated values are shown at various energies in Table II. The stopping power calculations were made using I = 165 ev. According to private communication Bichsel has used a value of I = 175 ev.[74] More precise data points will be determined in the future by computor analysis.

From equation (20)

$$S_a = F_1(\beta_a) F_2(\beta_a) \frac{Z}{A} - F_2(\beta_a) \frac{Z}{A} \ln I_a' . \qquad (86)$$

$$\ln I_a' = F_1(\beta_a) - \frac{S_a}{F_2(\beta_a)} \frac{A}{Z} \qquad (87)$$

Also

$$\ln I_a' = \ln I_a + \text{Shell Corrections.} \qquad (88)$$

Thus,

$$\ln I_a = F_1(\beta_a) - \frac{S_a}{F_2(\beta_a)} \frac{A}{Z} - \text{Shell Corrections.} \qquad (89)$$

TABLE II

VALUES OF STOPPING POWER AT VARIOUS ENERGIES IN SILICON

Stopping Power	S_1	S_2	S_3	S_4	S_5	S_6
Proton Energy in Mev	159.75	149.75	144.56	139.23	133.70	128.00
Max. Possible Value*	4.2321	4.4070	4.4886	4.6324	4.7684	4.9084
Most Probable Value	4.2091	4.3759	4.4611	4.6061	4.7429	4.8833
Min. Possible Value**	4.1868	4.3459	4.4327	4.5791	4.7167	4.8575
Calculated Value	4.2330	4.4220	4.5288	4.6484	4.7809	4.9288
Calculated Bichsel Value	4.197	4.384	4.491	4.609	4.739	4.886

* Maximum Possible Value

** Minimum Possible Value

Since there is an uncertainty in S_a, there will also be an uncertainty in I. Table III lists the calculated values of ln I at specific proton energies. Calculated values[75] of the s he ll corrections were used.

TABLE III

VALUES OF THE LOGARITHM OF THE AVERAGE EXCITATION ENERGY OF SILICON AT VARIOUS PROTON ENERGIES

$\ln I_1$ E = 159.75 Mev	$\ln I_2$ E = 149.75 Mev	$\ln I_3$ E = 144.56 Mev	$\ln I_4$ E = 139.23 Mev	$\ln I_5$ E = 133.70 Mev	$\ln I_6$ E = 128.00
5.1273*	5.1688*	5.1968*	5.1453*	5.1309*	5.1482*
5.0880	5,1185	5.1505	5,1027	5,0909	5,1103
5.0474**	5,0665**	5.1058**	5.0611**	5.0520**	5.0734**

ln I is plotted as a function of energy in Figure XVI.

Let

E = Energy of proton in ev as it enters the absorber,

V = Channel in which the pulse is stored,

V_v = Voltage per channel = 0.02045 volts,

V_v = Voltage of the pulse stored by the multichannel analyzer,

A = Amplification factor of the electronic system,

C = Capacitance of detector,

q = Charge of pulse created by total absorption of proton,

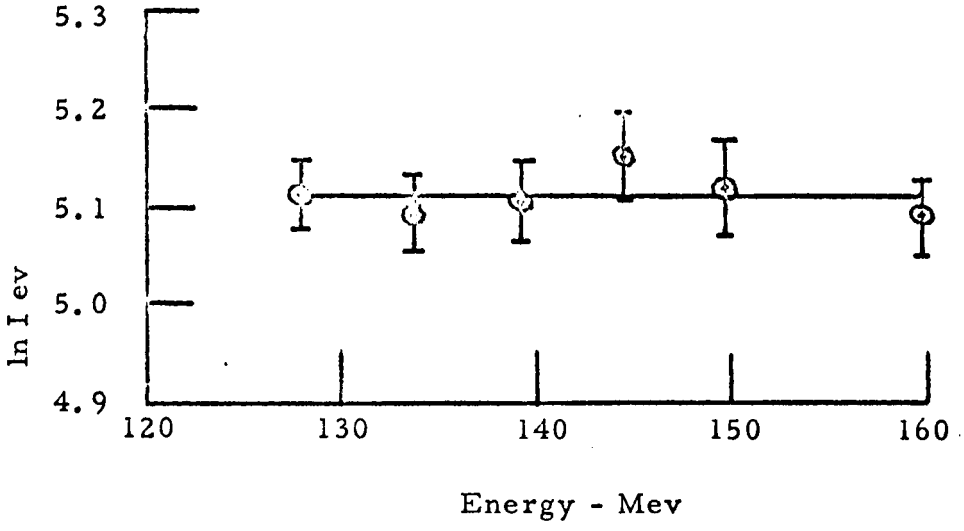

Fig. XVI. ln I for silicon as a function of proton energy

N = Average number of ion pairs created by absorption of proton of energy E_1,

e = 1.60206×10^{-19} coulombs,

p = Average energy in ev per ion pair = $\frac{E}{N}$.

$$V_v = q \frac{A}{C} . \tag{90}$$

$$q = Ne = E \frac{e}{p} \tag{91}$$

Substituting (91) into (90) yields

$$p = \frac{E e A}{C V_v} , \text{ or} \tag{92}$$

$$V_{mv} = \frac{e E_m A}{C p_m} \quad \text{where } m = 1, 2, 3 \text{ etc.} \tag{93}$$

Assuming $e \frac{A}{C}$ is constant, then

$$\frac{P_1}{P_2} = \frac{\frac{E_1}{V_1}}{\frac{E_2}{V_2}} = \frac{E_1 V_2}{E_2 V_1} . \tag{94}$$

Letting

$$V_m = V_c + \beta E_m \quad \text{and} \tag{95}$$

$$V_m - V_{m+1} = \beta (E_m - E_{m+1}) , \tag{96}$$

$$\beta = \frac{V_m - V_{m+1}}{E_m - E_{m+1}} . \qquad (97)$$

Case (1,2)

$$\beta = \frac{322.60 - 302.22}{159.75 - 149.75} = 2.0385$$

Case (1,3)

$$\beta = \frac{322.60 - 291.64}{119.75 - 144.56} = 2.0385$$

Solving (95) for V_o yields

$$V_0 = V_m - \beta E_m . \qquad (98)$$

$$V_o = 322.60 - 2.0385 \text{ X } 159.73$$

$$V_o = - 3.05$$

$$V_o = V_{m+1} - \beta E_{m+1} \qquad (99)$$

$$V_o = 302.22 - 2.0385 \text{ X } 149.75$$

$$V_{o} = - 3.05$$

$$p = \frac{159.75 \text{ X } 10^{6} \text{ X } 1.60206 \text{X } 10^{-19} \text{ X } 80.49}{90 \text{X } 10^{-12} \text{ X } 320.49 \text{ X } .02045} \qquad (100)$$

$$p = 3.49$$

$$\frac{P_1}{P_2} = \frac{159.75 \times 305.19}{149.75 \times 325.57} = 1.0000$$

$$\frac{P_1}{P_3} = \frac{159.75 \times 294.61}{144.56 \times 325.57} = 0.9999$$

$$\frac{P_1}{P_4} = \frac{159.75 \times 283.74}{139.23 \times 325.57} = 0.9999$$

Aluminum calibration data were used for the calculation of p_1.

DISCUSSION

The inversion layer formed during detector drift was formed by boron depletion from the "p" type surface. This phenomenon is well understood. It could be eliminated in future work by diffusing an outer ring of high concentration boron completely around the proposed lithium diffused area. A deep diffusion would be necessary in order that it not be etched off during future mesa etching. Boron concentrations above 10^{18} atoms/cm^3 effect a hole concentration high enough to prevent inversion. Thus, a guard ring is formed that would stop the inversion from spreading beyond that point.

Cleaner junctions exhibiting lower reverse leakage current could be prepared by the planar technique. By this method, a silicon dioxide layer is either thermally grown or vapor deposited on the silicon. This oxide layer could be masked by any means leaving the desired junction area uncoated. The silicon dioxide could be removed with hydrofluoric acid. During the lithium diffusion, the junction would be formed under the passivating layer which is extremely clean. No mesa etching would be required before or after the drift process. These two improvements would result in an excellent detector.

The 8 microampere reverse leakage current in addition to the 1500 volt operation with a 40:1 signal to noise ratio demonstrated the high quality of the mesa type detector. However, the drift parameter is appreciable at this voltage. Consequently, the device parameters will change with time. Also, the 5.8 mm sensitive region over a 12 cm length forms a very small solid angle for proton incidence. A series of round detectors with a 3 or 4 mm depletion layers could be stacked. The solid angle would be larger, a smaller operation voltage could be used, and the detector versatility would be greatly increased. Precise range studies could be made with this geometry.

The determined stopping power values, with possibly one exception, agree amazingly well with the theoretical ones. Data with this accuracy necessitated refined experimental technique. All reported values are accurate to four significant figures.

An average excitation energy of 166 ± 4 ev was determined. This differs slightly from the 175.0 ev calculated by Bichsel. According to the determinations it is, indeed, a constant.

Fair agreement was achieved with the accepted value of 3.6 ev electron-hole pair formation energy widely used in the literature.

CONCLUSION

The preparation and use of a lithium drifted semiconductor nuclear particle detector for total energy absorption is both feasible and desirable. Excellent agreement can be obtained between experimental and theoretical determinations of stopping power, average excitation energy and electron-hole pair formation energy for silicon. These values can be measured with extreme accuracy. An improved method of fabricating detectors and their use is proposed. This device would be of higher quality and could be employed with more versatility to make more and better measurements.

APPENDIX

From equation (61)

$$\frac{d^2V}{dx^2} = -\frac{\rho(x)}{k\epsilon_o} \quad . \tag{1}$$

From equation (60)

$$\rho(x) = -qax. \tag{2}$$

Substituting (60) into (61) yields

$$\frac{d^2V}{dx^2} = \frac{qax}{k\epsilon_o} \quad . \tag{3}$$

Integration yields

$$\frac{dV}{dx} = \frac{qax^2}{2k\epsilon_o} + K_1 \tag{4}$$

Integrating again, the voltage equation is obtained.

$$V = \frac{qax^3}{6k\epsilon_o} + K_1 x + K_2 \tag{5}$$

To evaluate the constant K_1, we make use of the assumption that all the applied voltage is dropped across the depletion region. In

other words, the electric field is zero outside the junction. Therefore, with the boundary conditions that $E = 0$ at $x = -x_m / 2$ and $x = +x_m / 2$ inserted into (4), K_1 becomes

$$K_1 = - \frac{q a x_m^2}{8 k \epsilon_o} , \qquad (6)$$

or

$$\frac{dV}{dx} = E = \frac{q a x^2}{2 k \epsilon_o} - \frac{q a x_m^2}{8 k \epsilon_o} \qquad \frac{-x_m}{2} \leq x \leq \frac{x_m}{2} . \qquad (7)$$

Equation (7) represents the way the electric field varies with distance through the depletion layer. Note that the field is maximum at $x = 0$.

$$E_{max} = \frac{- q a x_m^2}{8 k \epsilon_o} . \qquad (8)$$

The applied voltage V is equal to the potential V_n at $-x_m / 2$ less the potential V_p at $x_m / 2$.

$$V = V_n - V_p \qquad (9)$$

Evaluating equation (5) at the appropriate boundaries to obtain V_n and V_p yields

$$V(-\frac{x_m}{2}) = V_n = - \frac{q a x_m^3}{48 k \epsilon_o} - K_1 \frac{x_m}{2} + K_2 \qquad (10)$$

and

$$V\left(\frac{x_m}{2}\right) = V_p = \frac{q a x_m^3}{48 k \epsilon_o} + K_1 \frac{x_m}{2} + K_2 . \qquad (11)$$

Substituting equations (10) and (11) into (9) results in

$$V = - \frac{q a x_m^3}{24 k \epsilon_o} - K_1 x_m . \qquad (12)$$

Substituting equation (6) into equation (12) yields

$$V = \frac{q a x_m^3}{12 k \epsilon_o} . \qquad (13)$$

Solving for x_m,

$$x_m = \left[\frac{12 k \epsilon_o V}{q a} \right]^{1/3} \qquad (14)$$

For this same linear geometry, the capacitance per unit area is derived by utilizing

$$C = \frac{k \epsilon_o}{x_m} , \qquad (15)$$

which is the expression for the parallel-plate equivalent capacitance. Substituting equation (14) into equation (15) yields

$$C_T = \left[\frac{(k\epsilon_o)^2 q}{12} \right]^{1/3} \left(\frac{a}{V}\right)^{1/3} . \qquad (16)$$

BIBLIOGRAPHY

1. E. M. Pell, J. Appl. Phys. 31 (2), 291 (1960).

2. F. J. Morin and J. P. Maita, Phys. Rev. 96, 28 (1954).

3. C. S. Fuller and J. C. Severiens, Phys. Rev. 96 (1), 21 (1954).

4. H. Reiss, C. S. Fuller, and F. J. Morin, The Bell Sys. Tech. J. 35 (3), 535 (1956).

5. J. H. Elliot, Nucl. Inst. and Meth. 12 (1), 60 (1961).

6. E. M. Pell, Phys. Rev. 119, 1222 (1960).

7. H. Lawrence and R. M. Warner, Jr., The Bell Sys. Tech. J., 389 (1960).

8. G. Dearnaley and J. C. Lewis, Nucl. Inst. and Meth. 25, 237 (1964).

9. Charles Kittel, Introduction to Solid State Physics (John Wiley and Sons, New York, 1956), 2nd ed., Chap. 13.

10. Charles Kittel, Introduction to Solid State Physics (John Wiley and Sons, New York, 1956), 2nd ed., Appendix, 584.

11. Mendel Sachs, Solid State Theory (McGraw Hill, New York, 1963), 1st ed., Chap 7.

12. Mendel Sachs, Solid State Theory (McGraw Hill, New York, 1963), 1st ed., Chap. 7.

13. Crawford Dunlap, An Introduction to Semiconductors (John Wiley and Sons, New York, 1957), 1st ed., Chap. 11.

14. Mendel Sachs, Solid State Theory (McGraw Hill, New York, 1963), 1st ed., Appendix.

15. Crawford Dunlap, An Introduction to Semiconductors (John Wiley and Sons, New York, 1957), 1st ed., Chap. 5.

16. Mendel Sachs, Solid State Theory (McGraw Hill, New York, 1963), 1st ed., Chap. 6.

17. Crawford Dunlap, An Introduction to Semiconductors (John Wiley and Sons, New York, 1957), 1st ed., Chap. 11.

18. Charles Kittel, Introduction to Solid State Physics (John Wiley and Sons, New York, 1956), 2nd ed., Chap. 10.

19. F. J. Morin and J. P. Maita, Phys. Rev. 94, 1525 (1954).

20. W. Shockley, Electrons and Holes in Semiconductors (D. Van Nostrand, Princeton, N. J., 1953), 1st ed., Chap. 7.

21. Charles Kittel, Introduction to Solid State Physics (John Wiley and Sons, New York, 1956), 2nd ed., Chap. 13.

22. H. Reiss, C. S. Fuller, and F. J. Morin, The Bell Sys. Tech. J. 35 (3), 535 (1956).

23. M. Shashkov and I. P. Akimchenko, Soviet Phys. Doklady 4, 1115 (1959).

24. Charles Kittel, Introduction to Solid State Physics (John Wiley and Sons, New York, 1956), 2nd ed., Chap. 14.

25. Charles Kittel, Introduction to Solid State Physics (John Wiley and Sons, New York, 1956), 2nd ed., Chap. 10.

26. E. M. Conwell, Proc. IRE 46, 1281 (1958).

27. Crawford Dunhap, An Introduction to Semiconductors (John Wiley and Sons, New York, 1957), 1st ed., Chap. 5 and 8.

28. Richard Bube, Photoconductivity of Solids (John Wiley and Sons, New York, 1960), 1st ed., Chap. 3.

29. W. Shockley, Electrons and Holes in Semiconductors (D. Van Nostrand, Princeton, N. J., 1953), 1st ed., p. 287.

30. E. M. Conwell, Proc. IRE 40, 1331 (1952).

31. E. M. Conwell and V. F. Weisskopf, Phys. Ref. 77, 388 (1950).

32. G. W. Ludwig and R. L. Watters, Phys. Rev. 101, 1699 (1956).

33. M. B. Prince, Phys. Rev. 92, 681 (1953).

34. M. B. Prince, Phys. Rev. 93, 1204 (1954).

35. G. Backenstoss, Phys. Rev. 108, 1416 (1957).

36. Crawford Dunlap, An Introduction to Semiconductors (John Wiley and Sons, New York, 1957), 1st ed., Chap. 11.

37. Crawford Dunlap, An Introduction to Semiconductors (John Wiley and Sons, New York, 1957), 1st ed., Chap. 11.

38. W. R. Runyan, Silicon Semiconductor Technology (McGraw-Hill, New York, 1965), 1st ed., Chap. 8.

39. R. H. Kingston, J. Appl. Phys. 27, 101 (1956).

40. J. Bardeen, Phys. Rev. 71, 649 (1947).

41. W. H. Brattain and J. Bardeen, The Bell Sys. Tech. J. 32, 1 (1953).

42. G. Bemski, Proc. IRE 46, 990 (1958).

43. R. N. Hall, Phys. Rev. 83, 228 (1951).

44. W. Shockley and W. T. Read, Jr., Phys. Rev. 87, 835 (1952).

45. R. N. Hall, Phys. Rev. 87, 387 (1952).

46. W. H. Brattain and J. Bardeen, The Bell Sys. Tech. J. 32, 1 (1953).

47. J. R. Haynes and W. Shockley, Phys. Rev. 75, 691 (1949).

48. John Crank, The Mathematics of Diffusions (Clarendon Press, Oxford, England, 1956), 1st ed., Chap. 1.

49. Crawford Dunlap, An Introduction to Semiconductors (John Wiley and Sons, New York, 1957), 1st ed., Chap. 8.

50. J. M. Taylor, Semiconductor Particle Detectors (Washington Butterworths, Washington, D. C., 1963), 1st ed., Chap 1.

51. W. Shockley, Electrons and Holes in Semiconductors (D. Van Nostrand, Princeton, N. J., 1953), 1st ed., p. 318.

52. C. S. Fuller and J. C. Severiens, Phys. Rev. 96, 21 (1954).

53. J. P. Maita, J. Phys. Chem. Solids 4, 1546 (1958).

54. C. S. Fuller and J. A. Ditzenberger, Phys. Rev. 91, 193 (1953).

55. E. M. Pell, Phys. Rev. 119, 1222 (1960).

56. W. R. Runyan, Silicon Semiconductor Technology (McGraw-Hill, New York, 1965), 1st ed., Chap. 7.

57. G. Backenstoss, The Bell Sys. Tech. J., 37 (3), 699 (1958).

58. Crawford Dunlap, An Introduction to Semiconductors (John Wiley and Sons, New York, 1957), 1st ed., Chap. 8.

59. W. Shockley, Electrons and Holes in Semiconductors (D. Van Nostrand, Princeton, N. J., 1953), 1st ed., p. 461.

60. K. G. McKay and K. B. McAfee, Phys, Rev. 91, 1079 (1953).

61. K. G. McKay, Phys. Rev. 94, 877 (1954).

62. R. L. Pritchard, G. E. Research Lab. Report No. 57-RL-1817 (1957).

63. H. Lawrence and R. M. Warner, Jr., The Bell Sys. Tech. J. 39, 394 (1960).

64. H. Lawrence and R. M. Warner, Jr., The Bell Sys. Tech. J. 39, 395 (1960).

65. G. L. Miller, W. M. Gibson, and P. F. Donovan, Annual Rev. of N. Sc. 12, 194 (1962).

66. J. L. Blankenship and C. J. Barkowski, I. R. E. Trans. on N. Sc. 7, 183 (1960).

67. J. L. Blankenship and C. J. Barkowski, I. R. E. Trans. on N. Sc. 7, 184 (1960).

68. J. L. Blankenship and C. J. Barkowski, I. R. E. Trans. on N. Sc. 7, 181 (1960).

69. J. M. Taylor, Semiconductor Particle Detectors (Washington Butterworths, Washington, D. C., 1963), 1st ed., Chap. 4.

70. J. M. Taylor, Semiconductor Particle Detectors (Washington Butterworths, Washington, D. C., 1963), 1st ed., Chap 4.

71. W. H. Fonger, Noise in Electrical Devices (John Wiley and Sons, New York, 1957), 1st ed., Chap. 1.

72. A. Van Der Ziel, Fluctuation Phenomena in Semiconductors (Butterworths, London, England, 1959), 1st ed., Chap 2.

73. N. Bohr, Kgl. Danske Videnskab. Selskab. Mat. Fys. Medd. 18, 8 (1948).

74. Private Conversation Between George Crawford and H. Bichsel.

75. M. C. Walske, Phys. Rev. 88, 59 (1952).

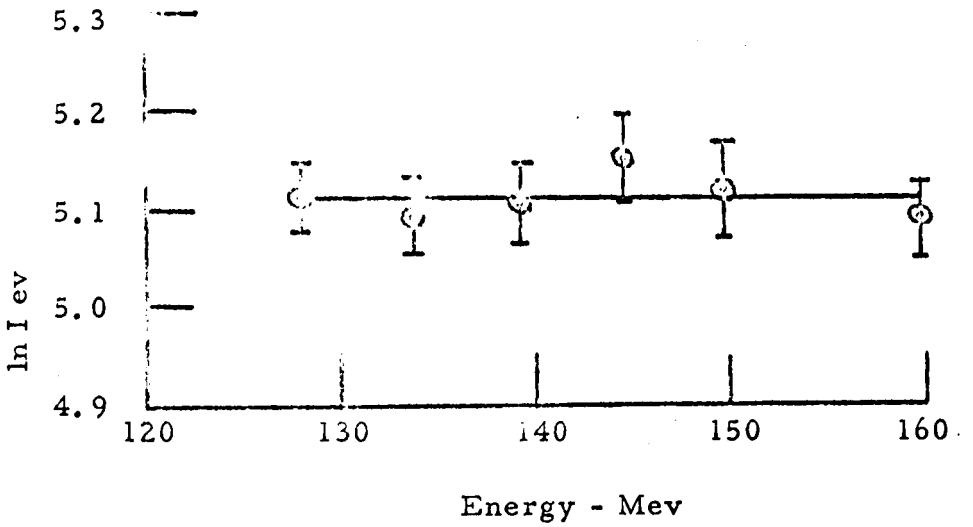

Fig. XVI. ln I for silicon as a function of proton energy